

Research



Article submitted to journal

Subject Areas:

xxxxx, xxxxx, xxxxx

Keywords:

Quantum optical models, pulsed twin beams, parametric down-conversion

Author for correspondence:

Alessandra Gatti

e-mail: Alessandra.Gatti@ifn.cnr.itUnified space-time description
of pulsed twin beamsAlessandra Gatti¹, Enrico Brambilla² and
Ottavia Jedrkiewicz^{1,2}¹Istituto di Fotonica e Nanotecnologie del CNR, Piazza
Leonardo da Vinci 32, 20133 Milano, Italy.²Dipartimento di Scienze e Alta Tecnologia, Università
dell'Insubria, Via Valleggio 11, 22100 Como, Italy

This work provides a mathematical derivation of a quasi-stationary model for multimode parametric down-conversion, which was presented in [Gatti *et al.*, *Sci. Rep.* 13, 16786] with heuristic arguments. The model is here derived from the 3D+1 propagation equation of the quantum fields in a nonlinear crystal, and its approximations discussed thoroughly. Thanks to its relative simplicity, and to the fact that it is valid in any gain regime, both at a quantum and classical level, it allows a unified description of disparate experimental observations conducted over the last 20 years, often described in the past by means of limited ad hoc models.

Introduction

During propagation in certain nonlinear materials, light photons from an intense optical beam can occasionally split into pairs of lower-energy photons, traditionally named “twins” because of their simultaneity [1]. Twin photons share not only the time of their birth, but essentially all their physical properties. In a quantum mechanical description, this implies that their state is nonseparable (*entangled*) with respect to all light degrees of freedom. Moreover, since the process is intrinsically broadband, twin photons can be generated in a large number of independent space-time modes [2–4]. These features made parametric down-conversion (PDC), as classically is called the process, a favorite choice for quantum imaging (see the reviews [5–7]), which exploits their spatial transverse entanglement, or entangled two-photon microscopy [8,9] and spectroscopy [10], which relies on their time-frequency correlation. However, the same features make the theoretical description of multimode PDC challenging. A well-known analytical model exists in the low-gain perturbative limit [11], see

also [12,13], in which photon pairs are individually generated and detected. Though, real-world implementations of quantum imaging and microscopy are likely to rather require the bright entangled beams (or the *bright squeezed vacuum* [14]) generated at high-gain. In this regime, an analytical model is available only for a plane-wave pump [15–19], which, besides being nonphysical, does not correspond to modern setups based on the use of short laser pulses. Several theoretical approaches were developed to account for the finite size of the laser pump, including numerical simulations of stochastic equations [18], generalized Bogoliubov relations in the space-time domain [18] or in the time-domain only [20] (see also [21] for a classical version of these equations), the integro-differential equations described in [22], and various kind of Schmidt-mode decompositions [14,23]. However, all these approaches, despite being potentially very accurate, still need important numerical treatments to extrapolate results.

In a recent work of ours [24] a substantially simpler and semi-analytic model was presented on the basis of heuristic arguments. In the present work, we derive the same *quasi stationary* model (or different form of the same model) in a more rigorous way from the quantum propagation equations of light in a nonlinear medium, and we discuss thoroughly the assumptions on which it is based. In order not to burden the formalism, we focus on the widely used type I quasi-degenerate PDC, in which twin photons are generated with the same polarization and close to the same frequency. Generalizations to other configurations are not difficult, but will be discussed elsewhere. In the second part of the work, we explore some of its predictions, in the framework of different experimental observations performed in the last 20 years. Although the model describes any gain regime of PDC, we focus on the high-gain, in which many disparate experimental observations, previously described by *ad hoc* models, often limited to time-only or space-only domains, can find a valid description within our model.

1. Quasi-stationary model for pulsed PDC

(a) Background and definitions

Our analysis starts from the equations that describe the propagation in a nonlinear $\chi^{(2)}$ medium of the quantum fields associated with an input pump beam, of central frequency ω_p , and with the down-converted signal of central frequency $\omega_s = \omega_p/2$. We assume paraxial propagation around a mean direction z (Fig.1), and introduce the operators:

$$\hat{A}_j(\vec{r}, t, z) = \int \frac{d^2\vec{q}}{2\pi} \int \frac{d\Omega}{\sqrt{2\pi}} e^{i\vec{q}\cdot\vec{r}} e^{-i\Omega t} \hat{A}_j(\vec{q}, \Omega, z) \quad j = s, p \quad (1.1)$$

where $\vec{r} = x\vec{e}_x + y\vec{e}_y$ is the position in the transverse plane, $\vec{q} = q_x\vec{e}_x + q_y\vec{e}_y$ is the transverse wave-vector, Ω is the frequency offset from the carriers, and dimensions are such that $\hat{A}_j^\dagger(\vec{r}, t, z)\hat{A}_j(\vec{r}, t, z)$ is a photon number per unit area and time. Their evolution along the slab is best described in an interaction picture in which the linear propagation in the medium, accounting for diffraction and dispersion at any order, is subtracted (see [19,25] for details), by setting

$$\hat{A}_j(\vec{q}, \Omega, z) = e^{ik_{zj}(\vec{q}, \Omega)z} \hat{a}_j(\vec{q}, \Omega, z), \quad \text{where} \quad k_{zj}(\vec{q}, \Omega) = \sqrt{k_j^2(\vec{q}, \Omega) - q^2}, \quad (1.2)$$

$k_j(\vec{q}, \Omega)$ being the wave-number of the j -th wave (it depends on the direction of propagation through \vec{q} only for the extraordinary wave). Then, the lowercase operators \hat{a}_j evolve slowly under the action of the nonlinear interaction.¹ In common implementations of PDC aimed at generating quantum states of light, the parametric gain is not too large, which justifies the undepleted pump approximation, in which $\hat{a}_p(\vec{q}, \Omega, z) = \hat{a}_p(\vec{q}, \Omega, 0)$ and the pump operator is substituted by a c-number field. By adopting a shorthand notation, in which

$$\vec{\xi} := (x, y, t), \quad \vec{w} := (q_x, q_y, \Omega), \quad (1.3)$$

¹Notice that for broadband PDC this approximation is far better than the usual slowly varying envelope approximation [26]

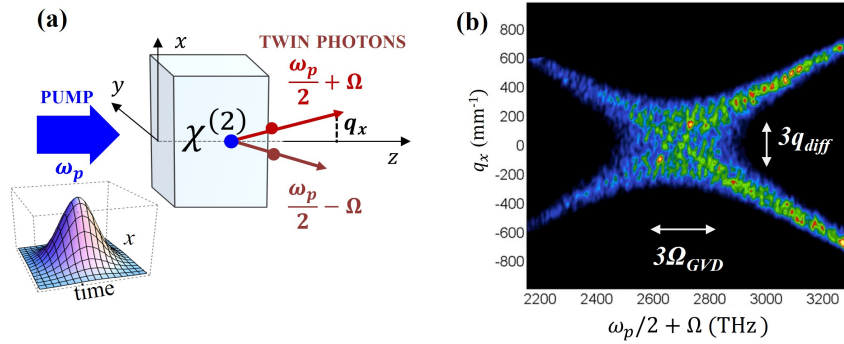


Figure 1. (a) Twin-photon generation in a $\chi^{(2)}$ medium. (b) Example of Fourier spectrum, measured in Ref. [27], generated from a 2 mm β -Barium borate (BBO) crystal pumped at 352 nm by a 1 ps, 200 μm FWHM pulsed beam. For these parameters the bandwidths, defined in Eq.(1.9), are $\Omega_{\text{GVD}} = 74$ THz, $q_{\text{diff}} = 86$ mm^{-1} .

with the convention for the scalar product: $\vec{w} \cdot \vec{\xi} = xq_x + yq_y - \Omega t$, the evolution of the signal field along the slab is described by the linear equation (see [18,19] for a derivation):

$$\frac{\partial \hat{a}_s}{\partial z}(\vec{w}, z) = \frac{g}{l_c} \int \frac{d^3 \vec{w}_0}{(2\pi)^{\frac{3}{2}}} \alpha_p(\vec{w}_0) \hat{a}_s^\dagger(\vec{w}_0 - \vec{w}, z) e^{-i\mathcal{D}(\vec{w}; \vec{w}_0 - \vec{w})z}, \quad (1.4)$$

where: $\alpha_p(\vec{w}) = \int \frac{d^3 \vec{\xi}}{(2\pi)^{\frac{3}{2}}} e^{-i\vec{w} \cdot \vec{\xi}} \alpha_p(\vec{\xi})$ is the Fourier profile of the input pump field, normalized so that $\alpha_p(\vec{\xi} = 0) = 1$; g is the dimensionless gain parameter, proportional to the nonlinear susceptibility, the crystal length and the pump peak amplitude;

$$\mathcal{D}(\vec{w}; \vec{w}_0 - \vec{w}) := k_{sz}(\vec{w}) + k_{sz}(\vec{w}_0 - \vec{w}) - k_{pz}(\vec{w}_0) \quad (1.5)$$

is the phase mismatch of the elementary process in which a pump photon in mode \vec{w}_0 splits into a photon pair in modes \vec{w} and $\vec{w}_0 - \vec{w}$, with conservation of the energy and transverse momentum.

(b) Quasi-stationary approximation

The solution of equation (1.4) is a generalized Bogoljubov transformation, similar to that studied in [18], linking in a nonlocal way operators at position z to those at the input $\hat{a}_s^{\text{in}}(\vec{w}) := \hat{a}_s(\vec{w}, 0)$:

$$\hat{a}_s(\vec{w}, z) = \int d^3 \vec{w}' \left[\mathcal{K}_1(\vec{w}, \vec{w}', z) \hat{a}_s^{\text{in}}(\vec{w}') + \mathcal{K}_2(\vec{w}, \vec{w}', z) \hat{a}_s^{\text{in}}(-\vec{w}') \right]. \quad (1.6)$$

where the kernels of the transformation obey the evolution equations

$$\begin{aligned} \frac{\partial \mathcal{K}_1}{\partial z}(\vec{w}, \vec{w}') &= \frac{g}{l_c} \int \frac{d^3 \vec{w}_0}{(2\pi)^{\frac{3}{2}}} \alpha_p(\vec{w}_0) \mathcal{K}_2^*(\vec{w}_0 - \vec{w}, -\vec{w}') e^{-i\mathcal{D}(\vec{w}; \vec{w}_0 - \vec{w})z} \\ \frac{\partial \mathcal{K}_2}{\partial z}(\vec{w}, \vec{w}') &= \frac{g}{l_c} \int \frac{d^3 \vec{w}_0}{(2\pi)^{\frac{3}{2}}} \alpha_p(\vec{w}_0) \mathcal{K}_1^*(\vec{w}_0 - \vec{w}, -\vec{w}') e^{-i\mathcal{D}(\vec{w}; \vec{w}_0 - \vec{w})z} \end{aligned} \quad (1.7)$$

with initial conditions $\mathcal{K}_1(\vec{w}, \vec{w}')|_{z=0} = \delta(\vec{w} - \vec{w}')$ and $\mathcal{K}_2(\vec{w}, \vec{w}')|_{z=0} = 0$.

Up to now we merely reformulated the propagation equation (1.4). A well-know solution exists in the limit of a monochromatic plane-wave pump (PWP) [15–19], $\alpha_p(\vec{w}_0) \rightarrow (2\pi)^{3/2} \delta(\vec{w}_0)$, in which the kernels reduce to Dirac-delta functions. The *quasi-stationary* approximation aims at going beyond the unphysical PWP limit, assuming that the pump pulse is finite but its Fourier spectrum is narrow enough that there exist two-well separated scales of variation:

– A *fast* scale, characterizing the decay of the coherence and correlation functions in the Fourier domain. An educated guess, based on the low gain perturbative solution, is that this scale is

associated with the Fourier spectrum of the pump. Indeed, energy-momentum conservation imposes that in the spontaneous regime, the energy and transverse momentum of twin photons sum up to the those of the pump beam. As we shall see, at high gain this fast scale undergoes some broadening [24,28,29].

– A *slow* scale, characterizing the decay of the overall Fourier spectrum of the PDC emission. This is associated with the scale of variation of the phase matching between conjugate modes:

$$l_c \mathcal{D}(\vec{w}; -\vec{w}) \approx l_c(2k_s - k_p) + \frac{\Omega^2}{\Omega_{\text{GVD}}^2} \text{sgn}(k_s'') - \frac{q^2}{q_{\text{diff}}^2} \quad (1.8)$$

where the Taylor expansion up to second order of Eq.(1.5) has been used, and

$$\Omega_{\text{GVD}} = |k_s'' l_c|^{-\frac{1}{2}}, \quad q_{\text{diff}} = \sqrt{k_s / l_c} \quad (1.9)$$

This scale, which reflects the conservation of longitudinal momentum in the parametric scattering, also undergoes a broadening at high gain [22,30].

Physically, this configuration corresponds to small correlated light speckles inside a broader spectral distribution, as observed in several high-gain experiments [22,27–29,31–34], and depicted in the example of Fig.1b. Mathematically, our derivation is based on two assumptions:

Ansatz 1 As a function of the difference $\vec{w} - \vec{w}'$, the kernels $\mathcal{K}_j(\vec{w}, \vec{w}')$ decay on the *fast* scale, and are non-zero over a restricted domain S_0 . As a function of \vec{w} (or \vec{w}' , or $\frac{\vec{w} + \vec{w}'}{2}$) they vary on the *slow* scale. As a consequence, for any $\vec{w}_0 \in S_0$ we can approximate $\mathcal{K}_j(\vec{w}, \vec{w}') = \mathcal{K}_j(\vec{w} + \vec{w}_0, \vec{w}' + \vec{w}_0)$ ².

Ansatz 2 For any $\vec{w}_0 \in S_0$ it holds the approximate identity:

$$\mathcal{D}(\vec{w}, \vec{w}_0 - \vec{w}) = \mathcal{D}(\vec{w}, -\vec{w}) - (k_p' - k_s') \Omega_0 - \frac{\partial k_p}{\partial q_x} q_{0x} \quad (1.10)$$

where we took the x axis in the direction of the walk-off of the Poynting vector ($\frac{\partial k_p}{\partial q_y} = 0$).

Notice that while the first ansatz is a very general statement, Ansatz 2 relies on the specific physical properties of the system. As discussed in Supplementary S.III, it can be obtained by retaining the dominant terms of the Taylor expansion of the phase mismatch in the fast variables \vec{w}_0 , and can be nicely satisfied provided that $\Omega_0 \ll \Omega_{\text{GVD}}$, $q_0 \ll q_{\text{diff}}$ (i.e. $\vec{w}_0 \in S_0$) and that the PDC bandwidth considered is not too large compared to Ω_{GVD} , see the example or Fig.S3.

Introducing the two ansatz in Eq.(1.7), the evolution equations for the kernels become:

$$\frac{\partial \mathcal{K}_1}{\partial z}(\vec{w}, \vec{w}') = \frac{g}{l_c} e^{-iD(\vec{w})z} \int \frac{d^3 \vec{w}_0}{(2\pi)^{\frac{3}{2}}} \alpha_p(\vec{w}_0) e^{i[(k_p' - k_s') \Omega_0 + \frac{\partial k_p}{\partial q_x} q_{0x}]z} \mathcal{K}_2^*(-\vec{w}, -\vec{w}' - \vec{w}_0) \quad (1.11)$$

where $D(\vec{w})$ is a shorthand for $\mathcal{D}(\vec{w}; -\vec{w})$. The equation for $\mathcal{K}_2(\vec{w}, \vec{w}')$ is obtained by exchanging $\mathcal{K}_1 \leftrightarrow \mathcal{K}_2$. These equations become more transparent if we introduce the Fourier transform of the kernels with respect to the difference of arguments (fast variable):

$$\mathcal{K}_j(\vec{w}, \vec{w}') = \int \frac{d^3 \vec{\xi}}{(2\pi)^3} e^{-i(\vec{w} - \vec{w}') \cdot \vec{\xi}} f_j(\vec{w}, \vec{\xi}) \quad (1.12)$$

After some not difficult passages, the equations for the functions f_j are obtained:

$$\begin{aligned} \frac{\partial f_1}{\partial z}(\vec{w}, \vec{\xi}) &= \frac{g}{l_c} \alpha_p \left(\vec{\xi} + \vec{\xi}_{\text{WO}} \frac{z}{l_c} \right) f_2^*(-\vec{w}, \vec{\xi}) e^{-iD(\vec{w})z} \\ \frac{\partial f_2^*}{\partial z}(-\vec{w}, \vec{\xi}) &= \frac{g}{l_c} \alpha_p^* \left(\vec{\xi} + \vec{\xi}_{\text{WO}} \frac{z}{l_c} \right) f_1(\vec{w}, \vec{\xi}) e^{iD(\vec{w})z} \end{aligned} \quad (1.13)$$

where $\vec{\xi}_{\text{WO}} = (-l_{\text{woff}}, 0, \tau_{\text{GVM}})$, with $l_{\text{woff}} = \frac{\partial k_p}{\partial q_x} l_c$ being the lateral walk-off between the pump and the signal in crossing the crystal, and $\tau_{\text{GVM}} = l_c(k_p' - k_s')$ the delay due to group velocity mismatch (GVM). In this way, we managed to reduce the completely coupled multimode problem

²In a truly stationary model, this would hold for any \vec{w}_0 not just in the fast domain S_0

(1.7) to a system of just two coupled equations for $f_1(\vec{w}, \xi)$ and $f_2(-\vec{w}, \xi)$, of much easier solution. Notice, that as long as $f_j(\vec{w}, \xi)$ are not flat functions of the space-time variable $\vec{\xi}$, these equations still couple a large number of PDC modes within the domain S_0 through the Bogoljubov transformation (1.6). Actually, for each fixed $\vec{\xi}$, equations (1.13) are two ordinary parametric equations, in which however the gain profile not only depends on $\vec{\xi}$, but also drifts along x and t while propagating, reflecting the spatial and temporal walk-off of the pump wave. Although it is not difficult to find complete solutions of Eqs. (1.13), this will be done elsewhere [35]. With the aim of deriving manageable results, in this work we make the more restrictive assumption:

$$\alpha_p(\vec{\xi} + \vec{\xi}_{\text{wo}} \frac{z}{l_c}) \simeq \alpha_p(\vec{\xi}) \quad (1.14)$$

The condition (1.14) should not be taken too strictly: as shown in [35], as long as the pump duration and cross section are not smaller than τ_{GVM} and l_{woff} , the effects of the spatio-temporal walk-off do not drastically change the picture, and can be accounted for by an effective gain parameter.

Assuming the validity of (1.14), the solution of Eqs.(1.13), with initial conditions $f_1(\vec{w}, \vec{\xi})|_{z=0} = 1$ and $f_2(\vec{w}, \vec{\xi})|_{z=0} = 0$, can be readily found. At the crystal exit face $z = l_c$ it reads:

$$f_j(\vec{w}, \vec{\xi}) \Big|_{z=l_c} = e^{-iD(\vec{w})\frac{l_c}{2}} F_j(\vec{w}, \vec{\xi}) \quad j = 1, 2, \quad \text{with} \quad (1.15)$$

$$F_1(\vec{w}, \vec{\xi}) = \cosh \Gamma(\vec{w}, \vec{\xi}) + i \frac{D(\vec{w})l_c}{2\Gamma(\vec{w}, \vec{\xi})} \sinh \Gamma(\vec{w}, \vec{\xi}),$$

$$F_2(\vec{w}, \vec{\xi}) = g\alpha_p(\vec{\xi}) \frac{\sinh \Gamma(\vec{w}, \vec{\xi})}{\Gamma(\vec{w}, \vec{\xi})}, \quad (1.16)$$

$$\Gamma(\vec{w}, \vec{\xi}) = \sqrt{|g\alpha_p(\vec{\xi})|^2 - \frac{[D(\vec{w})l_c]^2}{4}}.$$

Finally, the Bogoljubov transformation (1.6) can be recast in terms of these functions using Eq. (1.12) and (1.2). At $z = l_c$, it becomes the input-output relation:

$$\hat{A}_s^{\text{out}}(\vec{w}) = e^{i\phi(\vec{w})} \int \frac{d^3\vec{\xi}}{(2\pi)^{\frac{3}{2}}} e^{-i\vec{w}\cdot\vec{\xi}} \left[F_1(\vec{w}, \vec{\xi}) \hat{A}_s^{\text{in}}(\vec{\xi}) + F_2(\vec{w}, \vec{\xi}) \hat{A}_s^{\dagger \text{in}}(\vec{\xi}) \right] \quad (1.17)$$

where $\hat{A}_s^{\text{out}}(\vec{w}) = \hat{A}_s(\vec{w}, l_c)$, \hat{A}_s^{in} are vacuum input fields and

$$\phi(\vec{w}) = \frac{l_c}{2} [k_p + k_{sz}(\vec{w}) - k_{sz}(-\vec{w})] \quad (1.18)$$

Some remarks are in order:

- For the functions $F_j(\vec{w}, \vec{\xi})$, our Ansatz 1 translates into the requirement that they vary on the *slow scale* as functions of \vec{w} , while their Fourier transform with respect to $\vec{\xi}$ must decay on the *fast scale* (i.e. they are "fairly flat" functions of $\vec{\xi}$), so that $\int d^3\vec{\xi} F_j(\vec{w}, \vec{\xi}) e^{-i\vec{w}_0\cdot\vec{\xi}} \simeq \int d^3\vec{\xi} F_j(\vec{w} \pm \vec{w}_0, \vec{\xi}) e^{-i\vec{w}_0\cdot\vec{\xi}}$. Since these functions depend on $\vec{\xi}$ only through the pump profile, and depend on \vec{w} only through $D(\vec{w})l_c$, as anticipated, it is necessary that the pump spectrum is narrow enough with respect to the phase matching bandwidths (1.9), but how much is enough, it depends on the parameter g (see Supplementary S.II for a discussion).
- As can be easily verified, $|F_1(\vec{w}, \vec{\xi})|^2 - |F_2(\vec{w}, \vec{\xi})|^2 = 1$. This ensures the unitarity of the transformation (1.17), but only within the limits imposed by our initial Ansatz, as discussed in Supplementary S.I.
- These results are essentially equivalent to those in the Appendix A of [18], but i) we did not make the narrow frequency band approximation used in [18] ii) consistently, the formalism is different as it is adapted to describe broadband PDC; iii) the approximations made have been clarified.

(c) Correlation and coherence functions

The input-output relation (1.17) can be used to calculate the two second order moments that for such a Gaussian process determine all the statistical properties of the PDC emission:

$$\begin{aligned}\Psi(\vec{w}, \vec{w}') &= \langle \hat{A}_s^{out}(\vec{w}) \hat{A}_s^{out}(\vec{w}') \rangle = e^{i[\phi(\vec{w}) + \phi(\vec{w}')] } \int \frac{d^3 \vec{\xi}}{(2\pi)^3} e^{-i(\vec{w} + \vec{w}') \cdot \vec{\xi}} F_1(\vec{w}, \vec{\xi}) F_2(\vec{w}', \vec{\xi}) \\ &\simeq e^{i[k_p + (\Omega + \Omega') k'_s] l_c} \int \frac{d^3 \vec{\xi}}{(2\pi)^3} e^{-i(\vec{w} + \vec{w}') \cdot \vec{\xi}} F_1(\vec{w}, \vec{\xi}) F_2(-\vec{w}, \vec{\xi})\end{aligned}\quad (1.19a)$$

$$\begin{aligned}G^{(1)}(\vec{w}, \vec{w}') &= \langle \hat{A}_s^{\dagger out}(\vec{w}) \hat{A}_s^{out}(\vec{w}') \rangle = e^{i[\phi(\vec{w}') - \phi(\vec{w})]} \int \frac{d^3 \vec{\xi}}{(2\pi)^3} e^{-i(\vec{w}' - \vec{w}) \cdot \vec{\xi}} F_2(\vec{w}, \vec{\xi}) F_2^*(\vec{w}', \vec{\xi}) \\ &\simeq e^{i(\Omega' - \Omega) k'_s l_c} \int \frac{d^3 \vec{\xi}}{(2\pi)^3} e^{-i(\vec{w}' - \vec{w}) \cdot \vec{\xi}} |F_2(\vec{w}, \vec{\xi})|^2,\end{aligned}\quad (1.19b)$$

where F_1 and F_2 are given by Eq.(1.16). As expected, the biphoton amplitude $\Psi(\vec{w}, \vec{w}')$, defining the probability amplitude of finding an entangled photon pair in modes \vec{w} and \vec{w}' is peaked at $\vec{w}' = -\vec{w}$. Conversely, the coherence function $G^{(1)}(\vec{w}, \vec{w}')$ is peaked at $\vec{w}' = \vec{w}$. Coherently with the requirement of Ansatz 1, the correlation and coherence peaks decay on the *fast scale*, so that the second lines [Eqs.(1.19a) and (1.19b)] approximately hold (see also the discussion after Eq.(1.17)). The phases $\phi(\vec{w}') \pm \phi(\vec{w})$ were also approximated retaining only the dominant terms in the fast variable $\vec{w}' \pm \vec{w}$, in agreement with our Ansatz 2. One can easily recognize that these phase factors simply accounts for the finite time $k'_s l_c$ taken by the light pulses to cross the medium; in what follows we get rid of them by redefining $t = 0$ as the time at which the pump pulse *exits* the medium (notice that because of the assumption (1.14) this model is not able to account for any GVM delay).

The results in Eqs. (1.19a) and (1.19b) can be used in this form to calculate all the properties of the fluorescence emission at any gain. However a further very useful simplification can be performed. Focusing for example on the coherence function (1.19b), in order to study the mutual coherence as a function of the difference between arguments $\vec{w}_0 = \vec{w}' - \vec{w}$, at a given \vec{w} , it would be tempting to consider a normalized “distribution” of the form:

$$\mu_{coh}(\vec{w}_0, \vec{w}) = \frac{G^{(1)}(\vec{w}, \vec{w} + \vec{w}_0)}{\int d^3 \vec{w}_0 G^{(1)}(\vec{w}, \vec{w} + \vec{w}_0)} = \int \frac{d^3 \vec{\xi}}{(2\pi)^3} e^{-i\vec{w}_0 \cdot \vec{\xi}} \frac{|F_2(\vec{w}, \vec{\xi})|^2}{|F_2(\vec{w}, 0)|^2} \quad (1.20)$$

As shown in detail in Supplementary S.III, in the quasi-stationary conditions this quantity basically do not depend on \vec{w} for all the modes within the phase-matching bandwidth, and can be replaced by its peak value at $D(\vec{w}) = 0$. Namely, we have:

$$\frac{|F_2(\vec{w}, \vec{\xi})|^2}{|F_2(\vec{w}, 0)|^2} \simeq \frac{\sinh^2 [g\alpha_p(\vec{\xi})]}{\sinh^2 g} := F_{coh}(\vec{\xi}), \quad (1.21)$$

and similarly:

$$\frac{F_1(\vec{w}, \vec{\xi}) F_2(-\vec{w}, \vec{\xi})}{F_1(\vec{w}, 0) F_2(-\vec{w}, 0)} \simeq \frac{\cosh [g\alpha_p(\vec{\xi})] \sinh [g\alpha_p(\vec{\xi})]}{\cosh g \sinh g} := F_{corr}(\vec{\xi}) \quad (1.22)$$

for all the modes \vec{w} within the phase matching bandwidth. In this way, the coherence and correlation functions assume the factorized form that was proposed, with heuristic arguments, in Ref. [24]:

$$\psi(\vec{w}, \vec{w}') = e^{ik_p l_c} F_1(\vec{w}, 0) F_2(-\vec{w}, 0) \int \frac{d^3 \vec{\xi}}{(2\pi)^3} e^{-i(\vec{w} + \vec{w}') \cdot \vec{\xi}} F_{corr}(\vec{\xi}), \quad (1.23a)$$

$$G^{(1)}(\vec{w}, \vec{w}') = |F_2(\vec{w}, 0)|^2 \int \frac{d^3 \vec{\xi}}{(2\pi)^3} e^{-i(\vec{w}' - \vec{w}) \cdot \vec{\xi}} F_{coh}(\vec{\xi}), \quad (1.23b)$$

where F_{corr} and F_{coh} are given by Eqs. (1.22) and (1.21). We notice that $F_1(\vec{w}, 0)$ and $F_2(\vec{w}, 0)$ coincide with the well known functions of the PWP solution [15], while the Dirac-delta correlation of the PWP model are now replaced by finite peaks:

$$\mu_\beta(\vec{w}_0) = \int \frac{d^3\vec{\xi}}{(2\pi)^3} e^{-i\vec{w}_0 \cdot \vec{\xi}} F_\beta(\vec{\xi}), \quad (\beta = corr, coh) \quad (1.24)$$

We remark that depending on the application both expressions (1.19) or (1.23) can be used: clearly, the latter form is more manageable for analytical calculations, due to its factorized form.

2. Connection with experimental observations

The quasi-stationary model derived in the previous section (hereinafter QS model) is approximate, but it has the advantage of describing, through relatively simple formulas, all aspects of parametric generation, both at a classical and quantum level and in any gain regime. In the following we present a (non-exhaustive) review of experimental observations of high-gain PDC performed in the last 20 years and of their connection with the QS model.

(a) Spectral properties (angle-frequency domain)

This section is devoted to the properties of parametric radiation in the Fourier domain, which in experiments corresponds to the angle-frequency domain.

Regarding the coherence and correlation peaks μ_β defined in Eq.(1.24), the QS model predicts a substantial broadening of their sizes for increasing gain. This was extensively discussed in [24] and is further detailed in Supplementary S.II. The highlight result (see Fig.S2) is that the coherence and correlation sizes in each direction of the Fourier space increase with gain proportionally to $\sqrt{\frac{g}{\tanh(g)}}$ and $\sqrt{\frac{2g}{\tanh(2g)}}$, respectively. Notice that, rather than the second order field moments (1.19), experiments typically measure the correlations of light intensity, which are connected to the former by the Gaussian factorization theorem: $\langle \delta \hat{I}(\vec{w}) \delta \hat{I}(\vec{w}') \rangle = \langle \hat{I}(\vec{w}) \rangle \delta(\vec{w} - \vec{w}') + |G^{(1)}(\vec{w}, \vec{w}')|^2 + |\Psi(\vec{w}, \vec{w}')|^2$, where $\delta \hat{I}(\vec{w}) = \hat{A}_s^{\dagger out}(\vec{w}) \hat{A}_s^{out}(\vec{w}) - \langle \hat{A}_s^{\dagger out}(\vec{w}) \hat{A}_s^{out}(\vec{w}) \rangle$. The first term represents the shot-noise, while the two other terms at r.h.s. correspond to the classical *auto-correlation* peak, centered at $\vec{w} = \vec{w}'$ and to a *cross-correlation* peak, centered at $\vec{w}' = -\vec{w}$, of purely quantum origin.

With the use of CCD cameras with their high pixel resolution, several experiments were able to detect the speckled spatial pattern of the radiation generated by high-gain PDC, realized by pumping a nonlinear crystal with pulses typically in the picosecond range. In [31] and [28] a first description of the spatial properties of PDC radiation emitted by a type II BBO crystal pumped by a Nd:glass laser (1ps, 20 Hz) was given. A huge number of radiation transverse modes was detected by means of a high quantum efficiency CCD camera placed in the far-field of the source. The single-shot signal and idler images revealed the speckle-pattern aspect of the far-field radiation, and directly showed an enlargement of the speckles dimensions (corresponding to the coherence area of PDC) as a function of the pump intensity, i.e. of the gain. Most importantly, this pioneering work allowed to experimentally demonstrate -for the first time to our knowledge- a sub-shot noise quantum correlation between a huge number of coupled transverse modes. As depicted by Fig.2c, the twin-beam character of spatial modes was demonstrated by measuring the variance of the photoelectron difference $n_s - n_i$ of the signal-idler symmetrical pixels versus the mean number $\langle n_s + n_i \rangle$ of the down-converted photons of the pixel-pair. As discussed in [28], the increase of the transverse coherence area with gain is associated with an increase of the transverse correlation area, as shown in Figs.2a and b. Then, as a consequence of this broadening, a transition from the quantum to the classical regime of the measured pixel by pixel correlation was observed [31], also confirmed by subsequent experiments performed by Brida et al. [32].

A systematic study of the transverse spatial coherence of high gain PDC was performed by Brida et al. in [33]. In that work, a substantial increase of the far-field coherence area with the mean

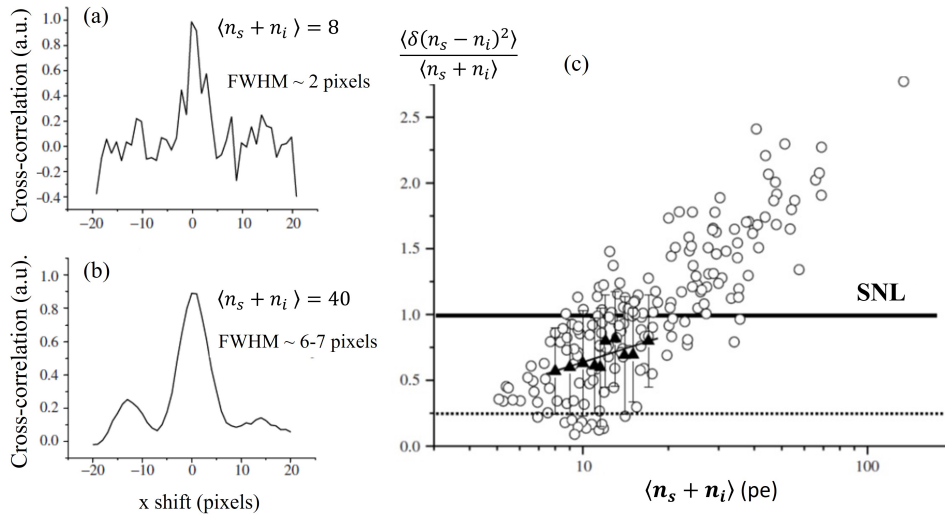


Figure 2. (a) and (b): Profile of the spatial cross-correlation of photon-numbers measured in [28], as a function of the transverse shift from symmetrical far-field positions; (c) The variance of the photon-number difference $n_s - n_i$ detected from symmetric signal-idler pixels, normalized to the shot noise $\langle n_s + n_i \rangle$ is plotted as a function of $\langle n_s + n_i \rangle$ [31].

number of detected PDC photons, in turn related to the gain, was observed, thus demonstrating that in high-gain the speckle size does not depend only on the pump diameter, as in the low-gain regime, but also on the pump intensity.

The coherence and correlation properties of twin beams were analysed deeply in [29]. This work characterized not only the angular features of twin beams, but also their spectral properties, thanks to the use of an imaging spectrometer placed in the far-field, as done in [36]. An example of a single-shot (θ, λ) spectrum of the twin beam radiation generated in a type I PDC process and recorded by an EMCCD camera, is reported in Fig. 3a, showing a speckled X-shaped spectrum. In [29] the changes of the angular-spectral radiation pattern with the pump power were investigated by evaluating the photon-number correlation coefficient. Figs. 3b and c clearly show the increase of the spectral and spatial FWHM size of the intensity autocorrelation (red circles) and cross-correlation (black circles) with increasing pump power, similarly to what observed in [37], where the spatio-spectral coherence properties of bright twin beam as a function of different pump beam parameters were investigated.

Regarding the angle-frequency spectrum, several works [21,22,30] highlighted that it broadens with increasing gain. This is also predicted by our QS model: by using Eqs.(1.23), it is indeed not difficult to provide an analytical (or semi-numerical) estimate of the spectral bandwidths, which is reported in Section S.II of Supplementary (Fig. S1). For instance, for type I collinear PDC the HWHMs of the intensity spectrum are approximately given by $\frac{\Delta\Omega}{\Omega_{\text{GVD}}} = \frac{\Delta q}{q_{\text{diff}}} = \sqrt[4]{\frac{4g^2 \log 2}{g \coth(g) - 1}}$ in the central part of the spectrum. In the arms of the X-spectrum, instead, one has a faster growth $\frac{\Delta\Omega}{\Omega_{\text{GVD}}} = \frac{\Delta q}{q_{\text{diff}}} = \frac{\Omega_{\text{GVD}}}{2\Omega_{\text{PM}}} \sqrt{\frac{4g^2 \log 2}{g \coth(g) - 1}}$, where $\Omega_{\text{PM}} \gg \Omega_{\text{GVD}}$ is the frequency at which phase-matching occurs. Notice that these formulas are obtained from the factorized form of the coherence function in Eq.(1.23), and as such they coincide with the results of the PWP model. If more refined results are needed, the less approximated formulas (1.19) can be used.

The dependence of the spectral bandwidth on the parametric gain was investigated in [30], for a range of g between 3.9 and 6.5 (below which the PDC signal was too low to be measured). In that setup, a BBO crystal was pumped at 354.7 nm by the third harmonic of a Nd:Yag laser, and the pump pulse had 18 ps duration and up to 0.1 mJ energy. The behaviour reported in Fig. 4a

shows the expected broadening of the emitted spectrum of the radiation with the parametric gain. Clearly, from the reported data it is not possible to say whether the grow rate is the $\sim \sqrt[4]{g}$ predicted by our QS model, and it would be interesting to verify with the authors of [30]. In the angular domain, a broadening of the spatial distribution of the far-field radiation and of the biphoton amplitude was observed and quantified in [22], where the authors also developed a theoretical-numerical approach to describe the features of high-gain PDC in the purely spatial domain. Fig. 4b, taken from [22], reports e.g. the evolution of the FWHM of the angular intensity distribution of the fluorescence with gain, measured in a experimental setup similar to that of [30]. Recent experiments showing the broadening of the far-field intensity profile and of the wavelength spectrum with increasing gain, are reported in [21].

(b) Space-time properties

This section is devoted to the properties of the fluorescence radiation in the complementary space-time domain, typically observed by imaging the crystal output plane [25,34].

By Fourier anti-transforming the correlation and coherence (1.23) of the QS model, one obtains:

$$\psi(\vec{\xi}, \vec{\xi}') = \langle \hat{A}_s^{out}(\vec{\xi}) \hat{A}_s^{out}(\vec{\xi}') \rangle = F_{corr}(\vec{\xi}) \int \frac{d^3 \vec{w}}{(2\pi)^3} e^{i\vec{w} \cdot (\vec{\xi}' - \vec{\xi})} F_1(\vec{w}, 0) F_2(-\vec{w}, 0), \quad (2.1a)$$

$$G^{(1)}(\vec{\xi}, \vec{\xi}') = \langle \hat{A}_s^{\dagger out}(\vec{\xi}) \hat{A}_s^{out}(\vec{\xi}') \rangle = F_{coh}(\vec{\xi}) \int \frac{d^3 \vec{w}}{(2\pi)^3} e^{i\vec{w} \cdot (\vec{\xi}' - \vec{\xi})} |F_2(\vec{w}, 0)|^2, \quad (2.1b)$$

The Fourier integrals at the r.h.s. represent space-time correlation and coherence peaks centered at $\vec{\xi}' = \vec{\xi}$ and fastly decaying with distance, which will be discussed at the end of this section. The slowly varying functions $F_{corr}(\vec{\xi})$ and $F_{coh}(\vec{\xi})$ defined by Eqs.(1.21) and (1.22) act as modulating envelopes. Then, F_{coh} provides the space-time distribution of the photon number at the crystal output plane, i.e. the transverse and temporal shape of the downconverted pulse. Conversely, F_{corr} is the biphoton amplitude, with $|F_{corr}|^2$ giving the probability distribution of finding two entangled photons at the space-time point $\vec{\xi}$. By simple analytical considerations, it is easy to show that F_{corr} and F_{coh} , which at low gain superimpose to the pump amplitude and intensity distribution, at high gain undergo a significant narrowing, with their width scaling in

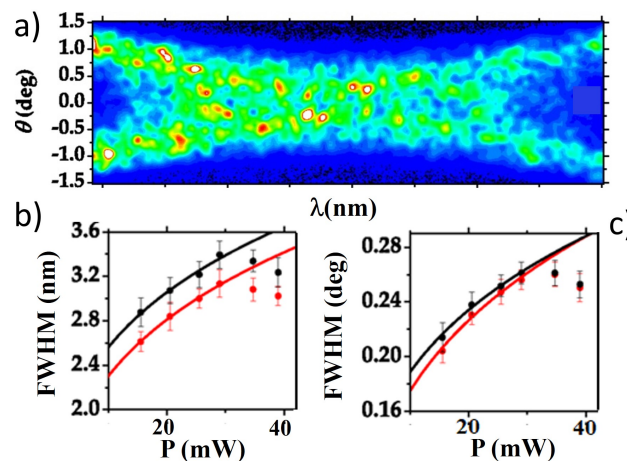


Figure 3. (a) Example of single shot (θ, λ) spectrum of the twin beams generated in a type I BBO crystal pumped by a 4.5 ps pulse at 349 nm; spectral (b) and angular (c) FWHM of the intensity autocorrelation (red circles) and cross-correlation (black circles) peaks as function of the pump power. The solid lines are a fit carried out for the first four data points under the assumption of undepleted pump beam [29].

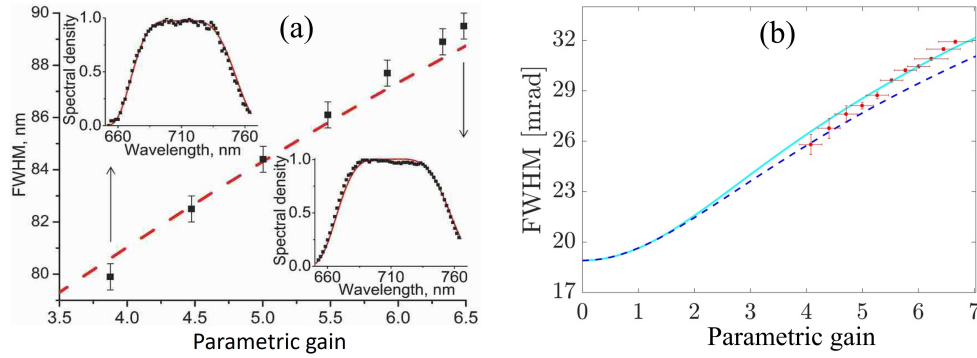


Figure 4. (a) Dependence of the PDC spectral width on the parametric gain (BBO crystal pumped at 354.7 nm with a 18 ps pulse). Insets show the shape of the spectrum at gain 3.9 and 6.5 respectively. Reprinted with permission from [30] ©Optical Society of America. (b) FWHM of the angular PDC spectrum reprinted from [22]. Experimental data (red points) are superimposed to the theoretical prediction of the spatial model (cyan curve) developed in [22] and of the PWP model (dashed curve).

each direction of space-time proportionally to $\sqrt{\frac{\tanh(2g)}{2g}}$ and $\sqrt{\frac{\tanh(g)}{g}}$, respectively (see Fig.5). Clearly, this narrowing of the distributions, already partially highlighted in Ref. [24], is nothing else than the counterpart of the broadening of the coherence and correlation peaks in the Fourier domain discussed in the previous section. To the best of our knowledge, the only experimental observations related to these aspects were reported by [38].

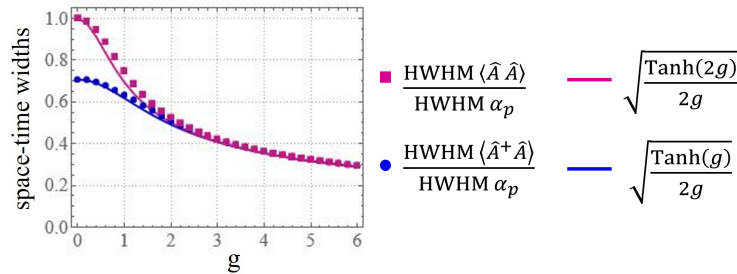


Figure 5. Theoretical widths HWHM of the photon-number distribution F_{coh} , (blue) and biphoton amplitude F_{corr} (purple), in space-time (see Eqs. (1.21) and (1.22)) as functions of g . The symbols are numerical evaluations, while the solid lines are analytical estimation from a Taylor expansion of the functions.

Regarding the space-time correlation and coherence, the Fourier integrals at the r.h.s. of Eqs.(2.1) are essentially the same results as the PWP model. These were analyzed in [27], for the classical coherence, and in [13,40] in the case of the quantum correlation. In these works, the characteristic X shape assumed in the space-time domain by the coherence and the correlation functions in proper conditions was highlighted, and the names “X-coherence” and “X-entanglement” were coined to underline the analogy with the X-waves of classical optics. The skewed nature in the space-time domain of the coherence was indirectly measured in [27], where the far-field X-spectrum in Fig.1b), characterized by chromatic and angular dispersion, was measured thanks to a spectral diagnostic technique based on an imaging spectrometer. These results, combined with the generalized form of the well-known Wiener-Kintchine theorem, clearly indicated that the physical origin of the X coherence relies on the phase-matching

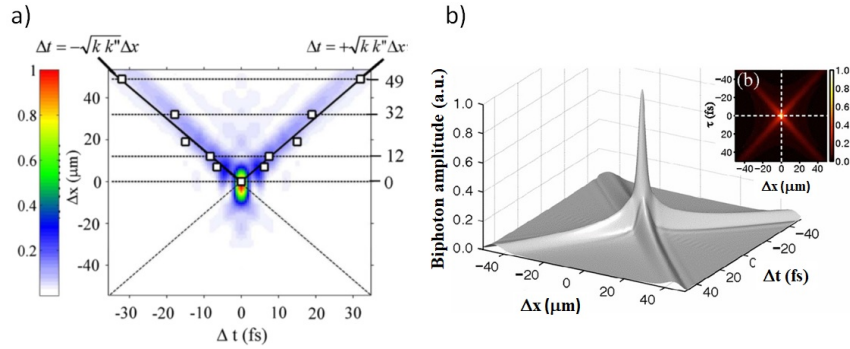


Figure 6. (a) Biphoton correlation $|\Psi(x, t; x + \Delta x, y + \Delta t)|$ measured by detecting the intensity of the SFG signal produced in a second crystal [25,39] as a function of a delay Δt and of a transverse shift Δx imposed on the twin beams. Due to the particular setup, only half of the X-shaped correlation was reproduced in the experiment. The experimental data points (open squares) are superimposed to a theoretical simulation of the experiment (density plot). Reprinted from [39]. The biphoton amplitude calculated [13] at the crystal output is shown in (b) for comparison.

conditions. The X-entanglement was instead directly experimentally detected [34,39], thanks to an interferometric-type scheme based on the inverse process of sum frequency generation (SFG) [25]. These works on the one side demonstrated the unusually narrow (6 fs FWHM) width of the quantum correlation [34], which is a consequence of the space-time non factorability [13] and reflects the high frequency-time entanglement of twin beams. On the other side, they demonstrated [39] the emission of entangled twin photons along the space-time skewed correlation trajectories depicted in Fig.6.

3. Conclusions

This work provides a mathematical derivation of a semi-analytical model for pulsed parametric fluorescence already presented in [24] without a derivation. The model is approximate, being based on an assumption of *quasi-stationarity*, but has the indisputable advantage of providing a simple and substantially analytical description of all the key aspects of the process, both at the classical and quantum levels, and in any gain regime. As such, we hope that it may represent a useful tool for researchers in the field. The more rigorous derivation of the QS model here performed allows to thoroughly inspect its limit of validity: essentially, for a transform-limited pump, the main requirements are that the pump duration be much longer than the temporal broadening $\sqrt{|k_s''|} l_c$ associated with group velocity dispersion (GVD) and at least on the same order as the group velocity delay $(k_p' - k_s') l_c$ between the two waves (see also the discussion in Supplementary S.II). Similarly, in the spatial domain it is necessary that the cross section of the pump is substantially larger than the diffraction broadening during propagation, and not smaller than the transverse walk-off between the two pulses. Then, in each specific configuration these conditions have to be checked (for instance for long crystals they are more difficult to meet, while close to the zero GVM or zero GVD points they are more easily satisfied), but they are usually met in common setups of high or medium-gain PDC, either quantum or classical, because these are also the conditions that ensure high efficiency of nonlinear conversion.

In the second part, we explore the main predictions of the model and we connect them to different experimental observations performed in the high-gain regime, where an analytical description was available only within the plane-wave pump approximation. The connection with the experiments is made by reviewing the properties of the PDC fluorescence measured in the frequency and angular (i.e. in the far field of the source) domains, and the space and time

properties typically observed by imaging the nonlinear crystal output plane.

This work focuses on type I quasi-degenerate PDC. Along the same lines, a quasi-stationary model can be easily formulated for type II or non-degenerate PDC, but we stress that the limits of validity of the model should be properly studied in each specific configuration.

Acknowledgements. The authors acknowledge support from the project PRIN 2022K3KMX7 of the MUR, ELISE "Enhancing multiphoton Light-matter Interactions with Space-time Entanglement", CUP B53D23005150006.

References

1. Burnham DC, Weinberg DL. 1970 Observation of Simultaneity in Parametric Production of Optical Photon Pairs. *Phys. Rev. Lett.* **25**, 84–87. ([10.1103/PhysRevLett.25.84](https://doi.org/10.1103/PhysRevLett.25.84))
2. Law CK, Walmsley IA, Eberly JH. 2000 Continuous Frequency Entanglement: Effective Finite Hilbert Space and Entropy Control. *Phys. Rev. Lett.* **84**, 5304–5307. ([10.1103/PhysRevLett.84.5304](https://doi.org/10.1103/PhysRevLett.84.5304))
3. Law CK, Eberly JH. 2004 Analysis and Interpretation of High Transverse Entanglement in Optical Parametric Down Conversion. *Phys. Rev. Lett.* **92**, 127903. ([10.1103/PhysRevLett.92.127903](https://doi.org/10.1103/PhysRevLett.92.127903))
4. Gatti A, Corti T, Brambilla E, Horoshko DB. 2012 Dimensionality of the spatiotemporal entanglement of parametric down-conversion photon pairs. *Phys. Rev. A* **86**, 053803. ([10.1103/PhysRevA.86.053803](https://doi.org/10.1103/PhysRevA.86.053803))
5. Gatti A, Brambilla E, Lugiato L. 2008 Chapter 5. Quantum imaging. , *Progress in Optics*, vol. 51, pp. 251–348. Elsevier. ([https://doi.org/10.1016/S0079-6638\(07\)51005-X](https://doi.org/10.1016/S0079-6638(07)51005-X))
6. Genovese M. 2016 Real applications of quantum imaging. *Journal of Optics* **18**, 073002. ([10.1088/2040-8978/18/7/073002](https://doi.org/10.1088/2040-8978/18/7/073002))
7. Moreau P, Toninelli E, Gregory T, J. PM. 2019 Imaging with quantum states of light. *Nature Reviews Physics* pp. 367–380. ([10.1038/s42254-019-0056-0](https://doi.org/10.1038/s42254-019-0056-0))
8. Tabakaev D, Montagnese M, Haack G, Bonacina L, Wolf JP, Zbinden H, Thew RT. 2021 Energy-time-entangled two-photon molecular absorption. *Phys. Rev. A* **103**, 033701. ([10.1103/PhysRevA.103.033701](https://doi.org/10.1103/PhysRevA.103.033701))
9. Raymer MG, Landes T, Marcus AH. 2021 Entangled two-photon absorption by atoms and molecules: A quantum optics tutorial. *Journal of Chemical Physics* **155**. ([10.1063/5.0049338](https://doi.org/10.1063/5.0049338))
10. Schlawin F, Dorfman KE, Mukamel S. 2018 Entangled Two-Photon Absorption Spectroscopy. *Acc. Chem. Res.* **51**, 2207–2214.
11. Ghosh R, Hong CK, Ou ZY, Mandel L. 1986 Interference of two photons in parametric down conversion. *Phys. Rev. A* **34**, 3962–3968. ([10.1103/PhysRevA.34.3962](https://doi.org/10.1103/PhysRevA.34.3962))
12. Atatüre M, Di Giuseppe G, Shaw MD, Sergienko AV, Saleh BEA, Teich MC. 2002 Multiparameter entanglement in femtosecond parametric down-conversion. *Phys. Rev. A* **65**, 023808. ([10.1103/PhysRevA.65.023808](https://doi.org/10.1103/PhysRevA.65.023808))
13. Gatti A, Brambilla E, Caspani L, Jedrkiewicz O, Lugiato LA. 2009 X-Entanglement: The Nonfactorable Spatiotemporal Structure of Biphoton Correlation. *Phys. Rev. Lett.* **102**, 223601. ([10.1103/PhysRevLett.102.223601](https://doi.org/10.1103/PhysRevLett.102.223601))
14. Sharapova P, Pérez AM, Tikhonova OV, Chekhova MV. 2015 Schmidt modes in the angular spectrum of bright squeezed vacuum. *Phys. Rev. A* **91**, 043816. ([10.1103/PhysRevA.91.043816](https://doi.org/10.1103/PhysRevA.91.043816))
15. Klyshko DN. 1988 *Photons and Nonlinear Optics*. New York: Gordon & Breach Science Pub.
16. Kolobov MI. 1999 The spatial behavior of nonclassical light. *Rev. Mod. Phys.* **71**, 1539–1589. ([10.1103/RevModPhys.71.1539](https://doi.org/10.1103/RevModPhys.71.1539))
17. Brambilla, E., Gatti, A., Lugiato, L. A., Kolobov, M. I. 2001 Quantum structures in traveling-wave spontaneous parametric down-conversion. *Eur. Phys. J. D* **15**, 127–135. ([10.1007/s100530170190](https://doi.org/10.1007/s100530170190))
18. Brambilla E, Gatti A, Bache M, Lugiato L. 2004 Simultaneous near-field and far-field spatial quantum correlations in the high-gain regime of parametric down-conversion. *Phys. Rev. A* **69**. ([10.1103/PhysRevA.69.023802](https://doi.org/10.1103/PhysRevA.69.023802))
19. Gatti A, Zambrini R, San Miguel M, Lugiato LA. 2003 Multiphoton multimode polarization entanglement in parametric down-conversion. *Phys. Rev. A* **68**, 053807. ([10.1103/PhysRevA.68.053807](https://doi.org/10.1103/PhysRevA.68.053807))

20. Christ A, Brecht B, Mauerer W, Silberhorn C. 2013 Theory of quantum frequency conversion and type-II parametric down-conversion in the high-gain regime. *New Journal of Physics* **15**, 053038. ([10.1088/1367-2630/15/5/053038](https://doi.org/10.1088/1367-2630/15/5/053038))
21. Kulkarni G, Rioux J, Braverman B, Chekhova MV, Boyd RW. 2022 Classical model of spontaneous parametric down-conversion. *Phys. Rev. Res.* **4**, 033098. ([10.1103/PhysRevResearch.4.033098](https://doi.org/10.1103/PhysRevResearch.4.033098))
22. Sharapova PR, Frascella G, Riabinin M, Pérez AM, Tikhonova OV, Lemieux S, Boyd RW, Leuchs G, Chekhova MV. 2020 Properties of bright squeezed vacuum at increasing brightness. *Phys. Rev. Res.* **2**, 013371. ([10.1103/PhysRevResearch.2.013371](https://doi.org/10.1103/PhysRevResearch.2.013371))
23. Wasilewski W, Lvovsky AI, Banaszek K, Radzewicz C. 2006 Pulsed squeezed light: Simultaneous squeezing of multiple modes. *Phys. Rev. A* **73**, 063819. ([10.1103/PhysRevA.73.063819](https://doi.org/10.1103/PhysRevA.73.063819))
24. Gatti A, Jedrkiewicz O, Brambilla E. 2023 Modeling the space-time correlation of pulsed twin beams. *Sci. Rep.* **13**, 16786. ([10.1038/s41598-023-42588-y](https://doi.org/10.1038/s41598-023-42588-y))
25. Brambilla E, Jedrkiewicz O, Lugiato LA, Gatti A. 2012 Disclosing the spatiotemporal structure of parametric down-conversion entanglement through frequency up-conversion. *Phys. Rev. A* **85**, 063834. ([10.1103/PhysRevA.85.063834](https://doi.org/10.1103/PhysRevA.85.063834))
26. Lugiato L, Prati F, Brambilla M. 2015 *Nonlinear Optical Systems*. Cambridge University Press. ([10.1017/CBO9781107477254](https://doi.org/10.1017/CBO9781107477254))
27. Jedrkiewicz O, Clerici M, Picozzi A, Faccio D, Di Trapani P. 2007 X-shaped space-time coherence in optical parametric generation. *Phys. Rev. A* **76**, 033823. ([10.1103/PhysRevA.76.033823](https://doi.org/10.1103/PhysRevA.76.033823))
28. Jedrkiewicz O, Brambilla E, Bache M, Gatti A, Lugiato LA, Trapani PD. 2006 Quantum spatial correlations in high-gain parametric down-conversion measured by means of a CCD camera. *Journal of Modern Optics* **53**, 575–595. ([10.1080/09500340500217670](https://doi.org/10.1080/09500340500217670))
29. Allevi A, Jedrkiewicz O, Brambilla E, Gatti A, Peřina J, Haderka O, Bondani M. 2014 Coherence properties of high-gain twin beams. *Phys. Rev. A* **90**, 063812. ([10.1103/PhysRevA.90.063812](https://doi.org/10.1103/PhysRevA.90.063812))
30. Spasibko KY, Iskhakov TS, Chekhova MV. 2012 Spectral properties of high-gain parametric down-conversion. *Opt. Express* **20**, 7507–7515. ([10.1364/OE.20.007507](https://doi.org/10.1364/OE.20.007507))
31. Jedrkiewicz O, Jiang YK, Brambilla E, Gatti A, Bache M, Lugiato LA, Di Trapani P. 2004 Detection of Sub-Shot-Noise Spatial Correlation in High-Gain Parametric Down Conversion. *Phys. Rev. Lett.* **93**, 243601. ([10.1103/PhysRevLett.93.243601](https://doi.org/10.1103/PhysRevLett.93.243601))
32. Brida G, Caspani L, Gatti A, Genovese M, Meda A, Berchera IR. 2009a Measurement of Sub-Shot-Noise Spatial Correlations without Background Subtraction. *Phys. Rev. Lett.* **102**, 213602. ([10.1103/PhysRevLett.102.213602](https://doi.org/10.1103/PhysRevLett.102.213602))
33. Brida G, Meda A, Genovese M, Predazzi E, Ruo-Berchera I. 2009b Systematic study of the PDC speckle structure for quantum imaging applications. *Journal of Modern Optics* **56**, 201–208. ([10.1080/09500340802464665](https://doi.org/10.1080/09500340802464665))
34. Jedrkiewicz O, Blanchet JL, Brambilla E, Di Trapani P, Gatti A. 2012 Detection of the Ultranarrow Temporal Correlation of Twin Beams via Sum-Frequency Generation. *Phys. Rev. Lett.* **108**, 253904. ([10.1103/PhysRevLett.108.253904](https://doi.org/10.1103/PhysRevLett.108.253904))
35. Gatti A. preprint Effects of spatio-temporal walk-off on pulsed parametric generation. alessandra.gatti@ifn.cnr.it.
36. Jedrkiewicz O, Picozzi A, Clerici M, Faccio D, Di Trapani P. 2006 Emergence of X-Shaped Spatiotemporal Coherence in Optical Waves. *Phys. Rev. Lett.* **97**, 243903. ([10.1103/PhysRevLett.97.243903](https://doi.org/10.1103/PhysRevLett.97.243903))
37. Allevi A, Lamperti M, Jedrkiewicz O, Galinis J, Machulka R, Haderka O, Peřina J, Bondani M. 2014 Spatio-spectral characterization of twin-beam states of light for quantum state engineering. *International Journal of Quantum Information* **12**, 1560027. ([10.1142/S0219749915600278](https://doi.org/10.1142/S0219749915600278))
38. Dickinson T, Caspani L, Clerici M et al.. 2023 Entangled two-photons interactions. Public seminar at Insubria University.
39. Jedrkiewicz O, Gatti A, Brambilla E, Di Trapani P. 2012 Experimental Observation of a Skewed X-type Spatiotemporal Correlation of Ultrabroadband Twin Beams. *Phys. Rev. Lett.* **109**, 243901. ([10.1103/PhysRevLett.109.243901](https://doi.org/10.1103/PhysRevLett.109.243901))
40. Caspani L, Brambilla E, Gatti A. 2010 Tailoring the spatiotemporal structure of biphoton entanglement in type-I parametric down-conversion. *Phys. Rev. A* **81**. ([10.1103/PhysRevA.81.033808](https://doi.org/10.1103/PhysRevA.81.033808))

41. Gurzadian G, Dmitriev V, Nikogosian D. 1997 *Handbook of Nonlinear Optical Crystals*. Springer series in optical sciences. Springer.
42. Pérez AM, Spasibko KY, Sharapova PR, Tikhonova OV, Leuchs G, Chekhova MV. 2015 Giant narrowband twin-beam generation along the pump-energy propagation direction. *Nature Communications* **6**. ([10.1038/ncomms8707](https://doi.org/10.1038/ncomms8707))

Appendix: Supplementary Material

This supplementary information investigates the range of validity of the approximations made in the main manuscript in order to derive the quasi-stationary model (hereinafter “QS model”) for multimode pulsed parametric down-conversion (PDC), and provides some specific examples, calculated in realistic PDC setups.

Section S.I investigates to what extent the quasi-stationary solution (1.17) of the propagation equation(1.4) defines a unitary transformation. Consistently, it shows that unitarity is satisfied only within the assumptions used to derive the model.

Section S.II studies the limit of validity of the Ansatz 1, which requires that the correlation and coherence decay in Fourier space on a much faster scale than the spectral bandwidths, using the results of the quasi-stationary model in Eqs.(1.23).

In section S.III we inspect the limit of validity of Ansatz 2 of the QS model [Eq.(1.10)], in which the generalized phase matching function $\mathcal{D}(\vec{w}; \vec{w}_0 - \vec{w})$ reduces to $\mathcal{D}(\vec{w}, -\vec{w}) - (k'_p - k'_s)\Omega_0 - \frac{\partial k_p}{\partial q_x} q_{0x}$.

The final section S.IV studies the validity of the approximations(1.21) and (1.22), by which the *quasi-stationary* biphoton correlation and the coherence function in Eq. (1.19) reduce to their factorized forms of Eqs.(1.23).

S.I Unitarity of the quasi-stationary solution of the propagation equation

In Sec.1(b) we found a solution of the linear propagation equation (1.4) by using a *quasi stationary approximation*, and wrote it as an-input output relation

$$\hat{A}_s^{out}(\vec{w}) = e^{i\phi(\vec{w})} \int \frac{d^3\vec{\xi}}{(2\pi)^3} e^{-i\vec{w}\cdot\vec{\xi}} \left[F_1(\vec{w}, \vec{\xi}) \hat{A}_s^{in}(\vec{\xi}) + F_2(\vec{w}, \vec{\xi}) \hat{A}_s^{\dagger in}(\vec{\xi}) \right] \quad (S1)$$

where \hat{A}_s^{in} are the input fields, and F_1 , F_2 and ϕ are defined in Eqs (1.16) and (1.18). The fundamental commutation relation for the output field reads:

$$\left[\hat{A}_s^{out}(\vec{w}), \hat{A}_s^{\dagger out}(\vec{w}') \right] = e^{i[\phi(\vec{w}) - \phi(\vec{w}')] } \int \frac{d^3\vec{\xi}}{(2\pi)^3} e^{i(\vec{w}' - \vec{w})\cdot\vec{\xi}} \left[F_1(\vec{w}, \vec{\xi}) F_1^*(\vec{w}', \vec{\xi}) - F_2(\vec{w}, \vec{\xi}) F_2^*(\vec{w}', \vec{\xi}) \right] \quad (S2)$$

$$\xrightarrow{\text{Ansatz 1}} e^{i[\phi(\vec{w}) - \phi(\vec{w}')] } \int \frac{d^3\vec{\xi}}{(2\pi)^3} e^{i(\vec{w}' - \vec{w})\cdot\vec{\xi}} \left[|F_1(\vec{w}, \vec{\xi})|^2 - |F_2(\vec{w}, \vec{\xi})|^2 \right] \quad (S3)$$

$$= e^{i[\phi(\vec{w}) - \phi(\vec{w}')] } \int \frac{d^3\vec{\xi}}{(2\pi)^3} e^{i(\vec{w}' - \vec{w})\cdot\vec{\xi}} 1 = \delta(\vec{w} - \vec{w}') \quad (S4)$$

where the second line holds within the quasi-stationary approximation. Indeed, by reformulating Ansatz1 for the F_j , taking into account the definition (1.12) and that $F_j(\vec{w}, \vec{\xi}) = e^{iD(\vec{w})\frac{L_c}{2}} f_j(\vec{w}, \vec{\xi})$, it implies that the Fourier transforms of the $F_j(\vec{w}, \vec{\xi})$ with respect to $\vec{\xi}$ die out on the *fast scale*. Thus, the r.h.s of Eq.(S2) vanishes for $\vec{w}' - \vec{w}$ outside the fast domain S_0 , which allows us to replace $F_j(\vec{w}, \vec{\xi}) F_j^*(\vec{w}', \vec{\xi}) \simeq F_j(\vec{w}, \vec{\xi}) F_j^*(\vec{w}, \vec{\xi})$ under the integral in (S2). Finally, as can be easily checked, $|F_1(\vec{w}, \vec{\xi})|^2 - |F_2(\vec{w}, \vec{\xi})|^2 = 1$, so that the result (S4) holds. In a similar way:

$$\left[\hat{A}_s^{out}(\vec{w}), \hat{A}_s^{out}(\vec{w}') \right] = e^{i[\phi(\vec{w}) + \phi(\vec{w}')] } \int \frac{d^3\vec{\xi}}{(2\pi)^3} e^{i(\vec{w}' - \vec{w})\cdot\vec{\xi}} \left[F_1(\vec{w}, \vec{\xi}) F_2(\vec{w}', \vec{\xi}) - F_2(\vec{w}, \vec{\xi}) F_1(\vec{w}', \vec{\xi}) \right] \quad (S5)$$

$$\xrightarrow{\text{Ansatz 1}} e^{i[\phi(\vec{w}) + \phi(\vec{w}')] } \int \frac{d^3\vec{\xi}}{(2\pi)^3} e^{-i(\vec{w}' + \vec{w})\cdot\vec{\xi}} \left[F_1(\vec{w}, \vec{\xi}) F_2(-\vec{w}, \vec{\xi}) - F_2(-\vec{w}, \vec{\xi}) F_1(\vec{w}, \vec{\xi}) \right] = 0 \quad (S6)$$

where the last results comes from the fact that $D(\vec{w})$ is by definition an even function of \vec{w} , so that $F_j(-\vec{w}) = F_j(\vec{w})$

S.II Ansatz 1: slow and fast scales in Fourier domain.

This section studies the limit of validity of the Ansatz 1, which requires that the correlation and coherence decay in Fourier space on a much faster scale than the spectral bandwidths, using the results of the quasi-stationary model in Eqs.(1.23).

As for the bandwidths, we consider the two spectral distributions:

$$G^{(1)}(\vec{w}, \vec{w}) = \left\langle \hat{A}_s^{\dagger out}(\vec{w}) \hat{A}_s^{out}(\vec{w}) \right\rangle = |F_2(\vec{w}, 0)|^2 \mu_{coh}(0) \quad (S7)$$

$$\Psi(\vec{w}, -\vec{w}) = \left\langle \hat{A}_s^{out}(\vec{w}) \hat{A}_s^{out}(-\vec{w}) \right\rangle = F_1(\vec{w}, 0) F_2(-\vec{w}, 0) \mu_{corr}(0) \quad (S8)$$

The first one is the usual light spectrum (expressed in photon number per unit area and time), giving the probability density of finding a photon in the Fourier mode $\vec{w} = (\vec{q}, \Omega)$, i.e at frequency $\omega_s + \Omega$ and at external angles $\sin \theta_x = \frac{q_x}{(\omega_s + \Omega)/c}$, $\sin \theta_y = \frac{q_y}{(\omega_s + \Omega)/c}$. The second function is such that $|\Psi(\vec{w}, -\vec{w})|^2$ provides the joint probability distribution of finding two entangled photons in a correlation volume around the conjugate modes \vec{w} and $-\vec{w}$, i.e at frequencies $\pm\Omega$ and angles $\sin \theta_x = \frac{\pm q_x}{(\omega_s \pm \Omega)/c}$, $\sin \theta_y = \frac{\pm q_y}{(\omega_s \pm \Omega)/c}$. The two functions depend on the Fourier coordinates only via the phase-mismatch $\bar{D}(\vec{w}) = l_c D(\vec{w})$. By making a Taylor expansion of these functions in \bar{D} , taken as the independent variable, around their maxima located at $\bar{D} = 0$, one can approximate the decay of the spectral distributions around their peak values as Gaussian functions of the phase mismatch \bar{D} :

$$\frac{G^{(1)}(\vec{w}, \vec{w})}{\mu_{coh}(0) \sinh^2(g)} = 1 - \frac{g - \tanh(g)}{2g^2 \tanh(g)} \frac{\bar{D}^2}{2} + o(\bar{D}^2) \approx e^{-\frac{g - \tanh(g)}{4g^2 \tanh(g)} \bar{D}^2} \quad (S9)$$

$$\frac{|\Psi(\vec{w}, \vec{w})|}{\mu_{corr}(0) \sinh(g) \cosh(g)} = 1 - \frac{g - \tanh(g)}{2g^2 \tanh(2g)} \frac{\bar{D}^2}{2} + o(\bar{D}^2) \approx e^{-\frac{g - \tanh(g)}{4g^2 \tanh(2g)} \bar{D}^2} \quad (S10)$$

Finally, one can use the Taylor expansion of the phase mismatch (1.8) to evaluate the spectral widths in q and Ω . Introducing the scaled variables $\bar{\Omega} = \frac{\Omega}{\Omega_{GVD}}$ and $\bar{q} = \frac{q}{q_{diff}}$, the collinear phase-mismatch parameter $\bar{D}_0 = (2k_s - k_p)l_c$, and defining $\eta = \text{sgn}(k_s'')$, one has

$$\bar{D}(\vec{q}, \Omega) \simeq \bar{D}_0 - \bar{q}^2 + \eta \bar{\Omega}^2 + o(\bar{q}^2, \bar{\Omega}^2) = \begin{cases} \bar{q}_{pm}^2 - \bar{q}^2, & \text{for } \bar{q}_{pm} = \sqrt{\eta \bar{\Omega}^2 + \bar{D}_0} \in \mathbb{R} \\ \bar{\Omega}^2 - \bar{\Omega}_{pm}^2, & \text{for } \bar{\Omega}_{pm} = \sqrt{\eta(\bar{q}^2 - \bar{D}_0)} \in \mathbb{R} \end{cases} \quad (S11)$$

where either expression can be used, provided it is real. When e.g. $\eta > 0$, for *collinear phase matching* $\bar{D}_0 = 0$ both expressions are always defined, for *noncollinear phase matching* $\bar{D}_0 > 0$ one needs $\bar{q} > \sqrt{\bar{D}_0}$, while for *nondegenerate phase matching* $\bar{D}_0 < 0$ one needs $\bar{\Omega} > \sqrt{-\bar{D}_0}$. Focusing for example on Ω (the arguments for the transverse bandwidth are perfectly symmetric), at leading order in the distance from the phase-matching point $\Delta\bar{\Omega} = \bar{\Omega} - \bar{\Omega}_{pm}$ one has: $\eta \bar{D}(\vec{w}) = 2\bar{\Omega}_{pm} \Delta\bar{\Omega} + \Delta\bar{\Omega}^2 \rightarrow \Delta\bar{\Omega}^2$, for $\bar{\Omega}_{pm} \ll \Delta\bar{\Omega}$, and $\eta \bar{D}(\vec{w}) \rightarrow 2\bar{\Omega}_{pm} \Delta\bar{\Omega}$, for $\bar{\Omega}_{pm} \gg \Delta\bar{\Omega}$. Substituting in the Gaussian expansions (S9), one can readily evaluate the spectral bandwidth, for example the Half Width at Half Maximum (HWHM) of the photon number distribution (S9) as:

$$\left(\frac{\Delta\Omega}{\Omega_{GVD}} \right)_{\text{spectr}} = \begin{cases} \sqrt[4]{\frac{4g^2 \tanh(g) \log 2}{g - \tanh(g)}} & \text{for } \bar{\Omega}_{pm} \lesssim 1 \\ \frac{1}{2\bar{\Omega}_{pm}} \sqrt[2]{\frac{4g^2 \tanh(g) \log 2}{g - \tanh(g)}} & \text{for } \bar{\Omega}_{pm} \gg 1 \end{cases} \quad (S12)$$

The same Gaussian approximation provides the HWHM width of the modulus of the biphoton amplitude (S10):

$$\left(\frac{\Delta\Omega}{\Omega_{GVD}} \right)_{|\Psi|} = \begin{cases} \sqrt[4]{\frac{4g^2 \tanh(2g) \log 2}{g - \tanh(g)}} & \text{for } \bar{\Omega}_{pm} \lesssim 1 \\ \frac{1}{2\bar{\Omega}_{pm}} \sqrt[2]{\frac{4g^2 \tanh(2g) \log 2}{g - \tanh(g)}} & \text{for } \bar{\Omega}_{pm} \gg 1 \end{cases} \quad (S13)$$

The expressions for the transverse bandwidth are completely equivalent, provided one substitutes in the formulas $\frac{\Delta\Omega}{\Omega_{GVD}} \rightarrow \frac{\Delta q}{q_{diff}}$ and $\bar{\Omega}_{pm} \rightarrow \bar{q}_{pm}$. These results are plotted by panels (d) and

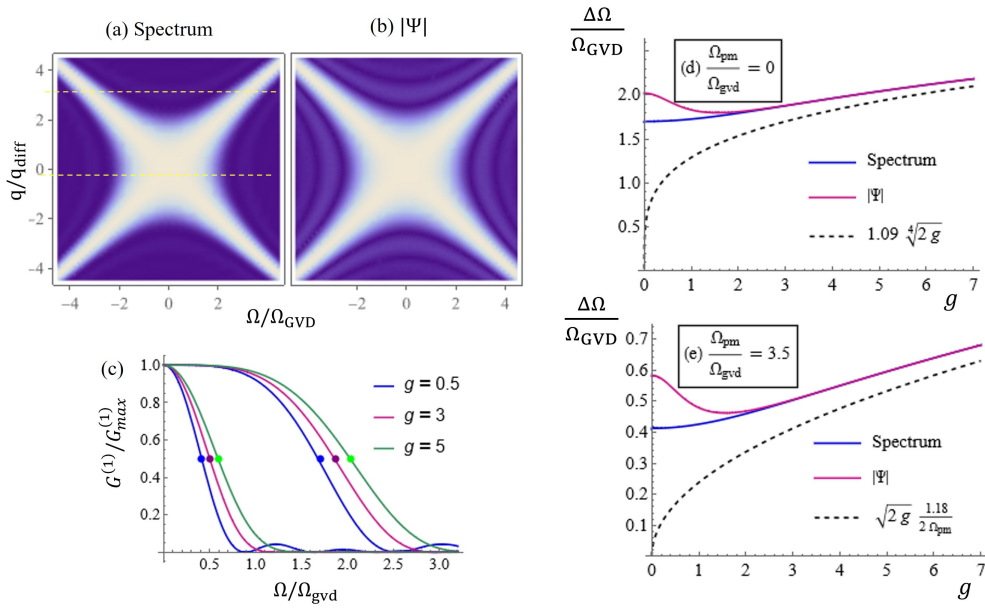


Figure S1. Spectral bandwidths. (a) and (b): Fourier distributions of the intensity $G^{(1)}(\vec{w}, \vec{w})$ and of the biphoton amplitude $|\Psi(\vec{w}, -\vec{w})|$, from Eqs.(S7) and (S8), respectively, evaluated using the Sellmeier relation in [41] for a 2mm BBO cut for collinear PDC from 515 \rightarrow 1030nm ($\bar{D}_0 = 0$), and for $g = 1$. (c): Sections of the intensity spectrum along the yellow dashed lines in (a), for three different values of the gain. The points are the HWHM evaluated from Eqs.(S12). (d) and (e) plot formulas (S12) and (S13) for the HWHM of the distributions, in (d) the central part of the spectrum $\Omega_{\text{pm}} = 0$, and e) in the arms, at $\Omega_{\text{pm}} = 3.5$. The dashed lines are the analytic asymptotes of the curves at large g , exhibiting a $\sqrt[4]{2g}$ and $\sqrt{2g}$ grow rate, respectively. The plots for the transverse bandwidths are identical, provided one substitutes $\frac{\Delta\Omega}{\Omega_{\text{gvd}}} \rightarrow \frac{\Delta q}{q_{\text{diff}}}$ and $\bar{\Omega}_{\text{pm}} \rightarrow \bar{q}_{\text{pm}}$. For these parameters $\Omega_{\text{gvd}} = 107$ THz, $q_{\text{diff}} = 71$ mm $^{-1}$.

(e) of Fig.S1. At low gain, the biphoton amplitude is broader than the intensity spectrum, reflecting the fact that in the spontaneous regime quantum correlated photons originate only from primary down-conversion processes. Therefore, the probability of finding entangled photon pairs $|\Psi(\vec{w}, \vec{w})|^2$ is distributed as the probability of finding single photons $G^{(1)}(\vec{w}, \vec{w})$, so that $|\Psi(\vec{w}, \vec{w})| \propto \sqrt{G^{(1)}(\vec{w}, \vec{w})}$ is broader than the intensity spectrum. Conversely, at high gain, also photon pairs that are not generated by the decay of the same pump photon can be quantum correlated as a consequence of cascaded stimulated processes, and contribute to the biphoton amplitude. Hence the two distributions tend to become identical as gain increases.

As observed by several experiments [22,30], both Fourier distributions broaden with increasing gain: our formulas show that the rate of broadening is different in the central part of the spectrum, where asymptotically the bandwidths grow as $g^{1/4}$, and along the thin arms of the X-shape, where they grow more rapidly as $g^{1/2}$. For comparison, the figure also plots the spectral distribution of the intensity (S7) (blue line) and biphoton amplitude (S8) (purple line), in the concrete example of a 2mm Beta-Barium-Borate (BBO) crystal, pumped for collinear (i.e. $\Delta_0 = 0$) down-conversion from 515 \rightarrow 1030nm, evaluated using the complete Sellmeier relation in [41]. In this example the crystal is cut for collinear and degenerate emission, but we remark that the results of Fig.S1d may also apply to noncollinear phase matching close to the degenerate frequency, while the plot in Fig. S1e also describes the widths along q for noncollinear phase matching at $q_{\text{pm}} = 3.5q_{\text{diff}}$, which for our parameters corresponds to an external emission angle ~ 2.34 degrees.

As for the widths of the correlation and coherence in the Fourier domain, we consider the normalized correlation peaks

$$\begin{aligned}\mu_{coh}(\vec{w}_0) &= \int \frac{d^3\xi}{(2\pi)^3} \frac{\sinh^2[g\alpha_p(\vec{\xi})]}{\sinh^2(g)} e^{-i\vec{w}_0 \cdot \vec{\xi}} \\ \mu_{corr}(\vec{w}_0) &= \int \frac{d^3\xi}{(2\pi)^3} \frac{\sinh[2g\alpha_p(\vec{\xi})]}{\sinh(2g)} e^{-i\vec{w}_0 \cdot \vec{\xi}}\end{aligned}\quad (S14)$$

Their widths were evaluated in our Ref. [24] as the mean square deviations $\sigma_{i,\beta}^2 = \int d^3\vec{w} w_i^2 \mu_\beta(\vec{w})$, ($i = q_x, q_y, \Omega$). By assuming a Gaussian pump of the form :

$$\alpha_p(r, t) = e^{-\frac{r^2}{w_p^2} - \frac{t^2}{\tau_p^2}} \quad (S15)$$

we obtained:

$$\sigma_{i,coh} = \sqrt{\frac{2g}{\tanh(g)}} \sigma_{i,pump}, \quad \sigma_{i,corr} = \sqrt{\frac{2g}{\tanh(2g)}} \sigma_{i,pump} \quad (S16)$$

where $\sigma_{i,pump}$ are the widths (root mean square deviation) of the pump Fourier amplitude along the Fourier coordinates: $\sigma_{q,pump} = \sqrt{2}/w_p$, $\sigma_{\Omega,pump} = \sqrt{2}/\tau_p$. Formulas (S16) are plotted in Fig.S2c, along with some examples of the profiles of the coherence peak (a) and of the correlation peak (b), for different gains. As known (see e.g. [13,40]), at low gain the biphoton correlation profile reproduces the Fourier profile of the pump *amplitude*, while the coherence peak is the Fourier transform of the pump *intensity*, and hence broader [for a Gaussian pump, $\alpha_p(\Omega) \sim \exp(-\frac{\Omega^2 \tau_p^2}{4})$, while the Fourier transform of the pump intensity $\sim \exp(-\frac{\Omega^2 \tau_p^2}{2})$]. At high gain the two profiles tend to coincide, because of the cross-talk between coherence and correlation arising from stimulated processes. They broaden with the gain, with an asymptotic behaviour $\sim g^{\frac{1}{2}}$. The lines with symbols in figure Fig.S2c show a numerical evaluation of the HWHM of the peaks, scaled to the HWHM of the pump Fourier profile. Were the peaks Gaussian, these curves would exactly match the solid lines in the plot. Instead, they are slightly below, because the correlation peaks have slowly decaying tails.

Part (d) of the figure shows instead the correlation width (HWHM of the peaks along the Ω_0 coordinate) scaled to the characteristic spectral bandwidth Ω_{GVD} , in the concrete example of collinear PDC in BBO (same parameters as in Fig.S1) and for three different pulse durations. By comparing with figure S1 we can conclude that it is not too difficult to satisfy the requirements of the quasi-stationary model (Ansatz1) when one considers the collinear and degenerate central part of the spectrum, whose width is on the order of $2\Omega_{GVD}$ (we remind that it grows slowly with the gain). In this case the requirement for a Gaussian pump pulse can be summarized as $\tau_p \gg \tau_{GVD} = \frac{1}{\Omega_{GVD}} = \sqrt{|k_s''' l_c|}$. In our example $\tau_{GVD} \simeq 6.6 - 21$ fs for crystal lengths 1 - 10 mm, and hence it is not difficult to fulfill the requirement for standard pulse durations. Clearly, in the case of a short pulse, the operating conditions must be carefully checked before adopting this model, especially when noncollinear phase matching is used, or when an ultra-broad part of the PDC spectrum, which also includes the thin arms of the "X", is taken into consideration.

The spatial aspects are completely equivalent and can be formulated in terms of $w_p \gg \frac{1}{q_{diff}} = \sqrt{\frac{l_c \lambda}{2\pi n_s}} \simeq 10 - 30 \mu\text{m}$. We do not discuss in detail the spatial aspects because there is normally no reason to use a tightly focused pulse for parametric generation in the quantum domain, since typically the gain required is not very high.

On the other hand, it is important to notice that the requirement made in Eq. (1.14), that the effects of walk-off and GVM are negligible, is typically more restrictive, as it implies that the pump duration and waist are larger or at least on the order of τ_{GVM} and l_{woff} , respectively. Then, the specific operational conditions should be checked: on the one side these quantities scale linearly with the crystal length. On the other, especially τ_{GVM} changes fast with the frequency. For example, for a BBO cut for collinear and degenerate phase matching $k'_p - k'_s$ ranges from 17 fs/mm for twin photons generated at 1300 nm, to 355 fs/mm for PDC at 704 nm (it is 92.8 fs/mm at 1030 nm). The

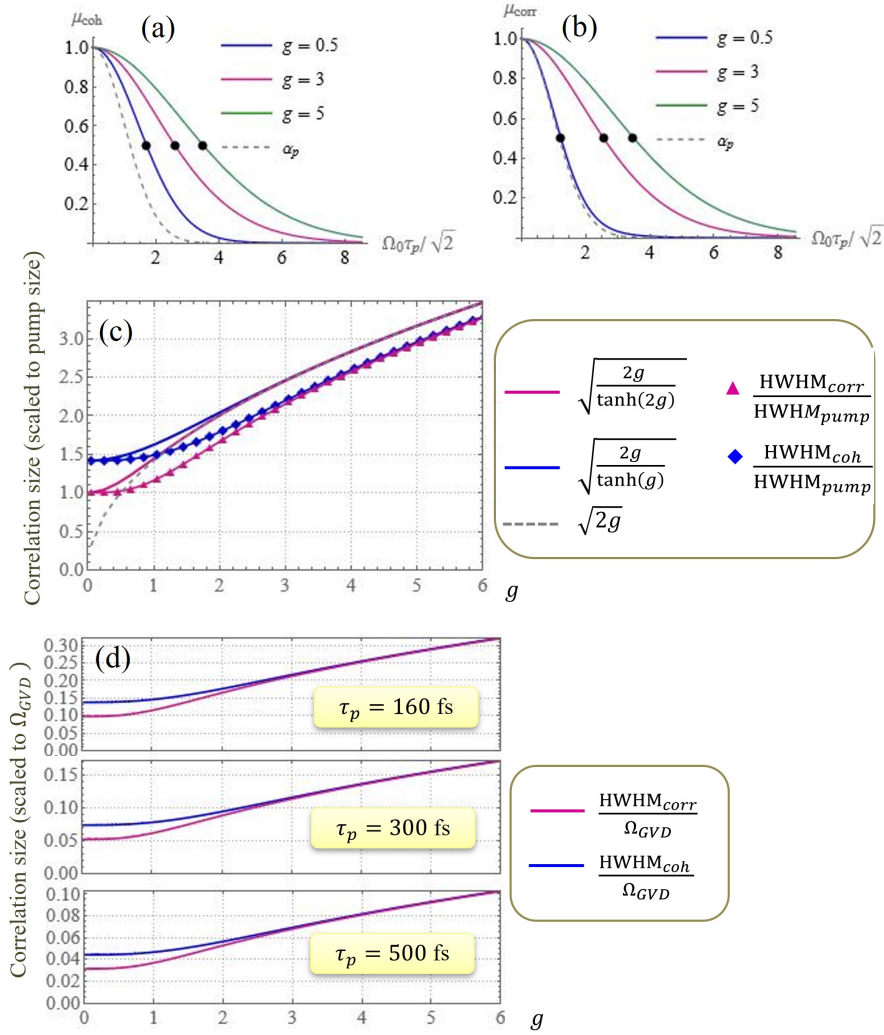


Figure S2. Correlation and coherence sizes. (a) and (b): Profile of the coherence and correlation peaks (S14), as a function of a Fourier coordinate, showing their broadening with increasing gain. (c) Plots the coherence (blue) and correlation (violet) widths, scaled to the pump width, as a function of the gain. The solid lines are formulas (S16), while the line with symbols are numeric evaluation of the HWHM of the peaks, scaled to the HWHM of α_p . (d) Show the correlation widths (HWHM of the peaks), scaled to the characteristic size of the PDC spectrum Ω_{GVD} , for three different pump pulse durations. Other parameters as in Fig.S1.

transverse walk-off length l_{woff} can be quite different for different materials and phase matching-conditions, ranging from ~ 0 for type 0 or non-critical phase-matching, to e.g. $\sim 60 \mu\text{m}/\text{mm}$ for PDC at 1030 nm from a BBO.

S.III Ansatz 2: Taylor expansion of phase matching in the fast variables

In this section we inspect the limit of validity of the Ansatz 2 to derive the quasi stationary solution, in which the phase matching function $\mathcal{D}(\vec{w}; \vec{w}_0 - \vec{w}) = k_{sz}(\vec{w}) + k_{sz}(\vec{w}_0 - \vec{w}) - k_{pz}(\vec{w}_0)$ is approximated as

$$\mathcal{D}(\vec{w}; \vec{w}_0 - \vec{w}) \xrightarrow{\text{Ansatz 2}} \mathcal{D}_{\text{appr}}(\vec{w}; \vec{w}_0 - \vec{w}) = \mathcal{D}(\vec{w}; -\vec{w}) - (k'_p - k'_s) \Omega_0 - \frac{\partial k_p}{\partial q_x} q_{0x} \quad (\text{S17})$$

for \vec{w}_0 belonging to the *fast* domain.

To this end, we expand the phase matching in Taylor series of the fast variable $\vec{w}_0 = (q_0x, q_0y, \Omega_0)$:

$$l_c[\mathcal{D}(\vec{w}; \vec{w}_0 - \vec{w}) - \mathcal{D}(\vec{w}; -\vec{w})] = l_c \left[\vec{\nabla} k_{sz}(-\vec{w}) - \vec{\nabla} k_{pz}(0) \right] \cdot \vec{w}_0 + o(q_0 l_{\text{woff}}, \Omega_0 \tau_{\text{GVM}}) \quad (\text{S18})$$

$$\simeq l_c (k'_s - k'_p - k''_s \Omega) \Omega_0 - l_c \left(\frac{\partial k_p}{\partial q_x} \vec{e}_x + \frac{\vec{q}}{k_s} \right) \cdot \vec{q}_0 \quad (\text{S19})$$

where in the second passage only the leading terms of the expansion of $\vec{\nabla} k_{sz}(-\vec{w})$ around $\vec{w} = 0$ (the central frequency and the collinear direction) have been retained. Here k'_j, k''_j are shorthands for $\frac{\partial k_j}{\partial \Omega}(\vec{w} = 0)$, $\frac{d^2 k_j}{d\Omega^2}(\vec{w} = 0)$, while $\frac{\partial k_p}{\partial q_x} \approx -\rho_p$ gives the *walk-off* angle of the Poynting vector of the extraordinary pump, assumed here in the x-direction. The quadratic terms neglected in Eq.(S19) are of the form $\frac{l_c}{2}(k''_s - k''_p)\Omega_0^2 \simeq \frac{\Omega_0^2}{2\Omega_{\text{GVD}}^2}$ and $\left(\frac{l_c}{2k_s} - \frac{l_c}{2k_p}\right)q_0^2 \simeq \frac{q_0^2}{4q_{\text{diff}}^2}$, where we remind that $\Omega_{\text{GVD}} = (|k''_s|l_c)^{-1/2}$ and $q_{\text{diff}} = (k_s/l_c)^{1/2}$ are the characteristic bandwidth of phase matching. Therefore, provided that the request of the quasi-stationary model are satisfied, i.e. that the correlation functions decay on distances $\Omega_0 \ll \Omega_{\text{GVD}}$, $q_0 \ll q_{\text{diff}}$ these terms can be safely neglected.

The term $l_c k''_s \Omega \Omega_0 = \frac{\Omega \Omega_0}{\Omega_{\text{GVD}}}$ becomes significant only when the spectral width of the correlation and of the coherence Ω_0 is larger than $\approx \Omega_{\text{GVD}} \frac{\Omega_{\text{GVD}}}{\Omega}$. Clearly, within the request of the quasi-stationary model, this term is negligible unless the PDC bandwidth considered is very large, so that $\frac{\Omega}{\Omega_{\text{GVD}}} \gg 1$.

For a tightly focused pump, the term $\frac{\vec{q} \cdot \vec{q}_0}{k_s}$ may originate the so-called *hot spots* [42], which are relevant only close to a specific angle $q_x/k_s = -\rho_p$ (for our BBO $\rho_p = -3.2^\circ$). In any case, this term is not negligible only when $q_0 \approx q_{\text{diff}} \frac{q_{\text{diff}}}{q}$, and within the quasi-stationary Ansatz 1, requires that broad angular bandwidth of PDC is considered.

Figure S3 provides a comparison between the full expression of phase mismatch and its approximate form (S17), in the example of a BBO cut for collinear and degenerate phase matching at 1030 nm. Panels (a) - (d) provide a visual comparison, showing density plots of the functions to be compared. Namely, (a) and (b) plot $\text{sinc}[\mathcal{D}(\vec{w}, \vec{w}_0 - \vec{w}) \frac{l_c}{2}]$ and $\text{sinc}[\mathcal{D}_{\text{appr}}(\vec{w}, \vec{w}_0 - \vec{w}) \frac{l_c}{2}]$, respectively, where $\mathcal{D}_{\text{appr}}(\vec{w}, \vec{w}_0 - \vec{w})$ is given by Eq.(S17), as functions of Ω (horizontal axis) and Ω_0 (vertical axis), for $q = q_0 = 0$. The red dashed lines enclose the region where the Fourier transform of a Gaussian pump of duration $\tau_p = 150 \text{ fs}$ is larger than $1/e$. (c) and (d) plot 2D cuts of the same functions along q and Ω_0 , for a $\Omega = 0$ and $q_0 = 0$. From these graphs it is possible to appreciate the validity of the approximation, at least in the central part of the PDC spectrum. In fact, unless the spectral widths of the correlation, which in the first instance we can approximate with those of the pump, are truly of the order or larger than Ω_{GVD} , the approximation is essentially an identity. Panel (e) shows a more quantitative comparison, plotting

$$\text{sinc}[\mathcal{D}_{\text{appr}}(\vec{w}, \vec{w}_0 - \vec{w}) \frac{l_c}{2}] - \text{sinc}[\mathcal{D}(\vec{w}, \vec{w}_0 - \vec{w}) \frac{l_c}{2}] \quad (\text{S20})$$

where the variables $\Omega_0 = 2/\tau_p$ and $q_0 = 2/w_p$ are the coordinates at which a Gaussian pump $\alpha_p(q_0, \Omega_0)$ reduces to $1/e$, and \vec{q} and Ω are chosen as to satisfy phase-matching for a plane-wave pump, i.e. $D(\vec{q}, \Omega) = 0$. Then, for $\vec{w}_0 = 0$, we have that $\text{sinc}[\mathcal{D}_{\text{appr}}(\vec{w}, -\vec{w}) \frac{l_c}{2}] = \text{sinc}[\mathcal{D}(\vec{w}, -\vec{w}) \frac{l_c}{2}] = 1$, and the quantity in Eq. (S20) is substantially the error normalized to unity. We notice that even in the case of the red and green curves, for which the pump duration and waist are rather small (i.e. the corresponding spectral widths are rather large), the error done with the approximation becomes appreciable only when $\Omega \geq 4\Omega_{\text{GVD}}$ in this example, that corresponds to a large PDC bandwidth $\sim 850 \text{ THz}$ or $\sim 500 \text{ nm}$ around $\lambda_s = 1030 \text{ nm}$.

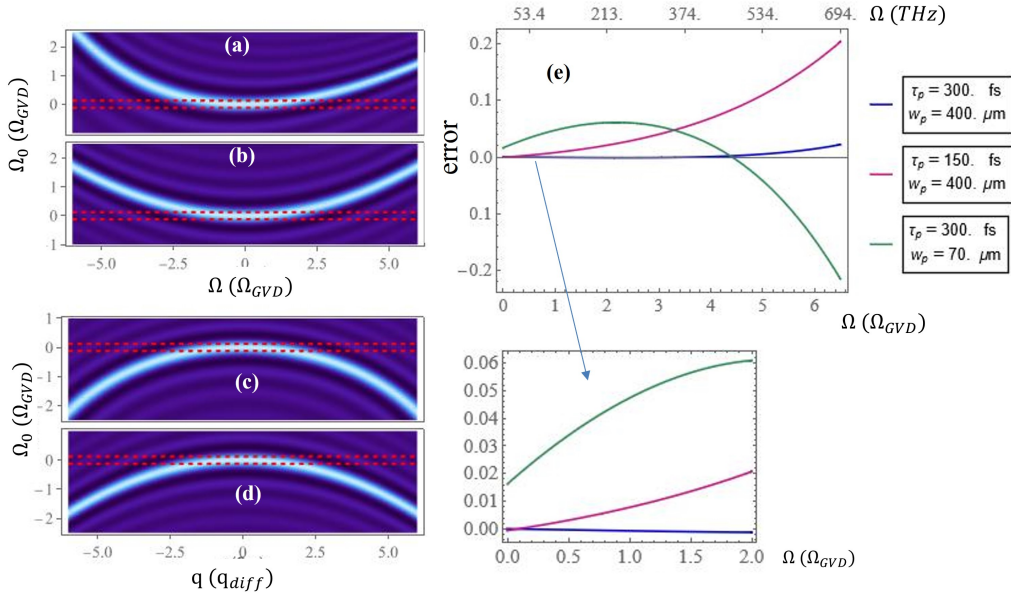


Figure S3. (a) and (b) compare $\text{sinc}[\mathcal{D}(\vec{w}, \vec{w}_0 - \vec{w}) \frac{L_c}{2}]$ and $\text{sinc}[\mathcal{D}_{\text{appr}}(\vec{w}, \vec{w}_0 - \vec{w}) \frac{L_c}{2}]$, with $\mathcal{D}_{\text{appr}}(\vec{w}, \vec{w}_0 - \vec{w})$ given by Eq.(S17), plotted as functions of Ω (horizontal axis) and Ω_0 (vertical axis), for $q = q_0 = 0$. The red dashed lines enclose the region where the Fourier transform of a Gaussian pump of duration $\tau_p = 150$ fs is larger than $1/e$. (c) and (d) are cuts of the same functions at $\Omega = 0$ and $q_0 = 0$. (e) Shows an estimate of the error, plotting $\text{sinc}[\mathcal{D}_{\text{appr}}(\vec{w}, \vec{w}_0 - \vec{w}) \frac{L_c}{2}] - \text{sinc}[\mathcal{D}(\vec{w}, \vec{w}_0 - \vec{w}) \frac{L_c}{2}]$, where \vec{q} and Ω are chosen to satisfy $D(\vec{q}, \Omega) = 0$, while $\Omega_0 = 2/\tau_p$ and $q_0 = 2/w_p$ are the coordinates at which a Gaussian pump $\alpha_p(q_0, \Omega_0) = 1/e$. Parameters are those of a 2mm BBO crystal, cut for collinear phase matching at 1030nm, as in FigS1.

S.IV Factorability of the quasi-stationary correlation and coherence functions.

This section studies the validity of the approximations (1.22) and (1.21), by which the *quasi-stationary* biphoton correlation and the coherence function in Eq. (1.19) reduce to their factorized forms reported by Eqs. (1.23).

The approximation is based on the observation that the kernels $F_1(\vec{w}, \vec{\xi})$, $F_2(\vec{w}, \vec{\xi})$ of the Bogoljubov relations (1.17) that solve the propagation equation in the quasi-stationary limit are such that the ratios

$$\frac{F_1(\vec{w}, \vec{\xi})}{F_1(\vec{w}, 0)}, \quad \frac{F_2(\vec{w}, \vec{\xi})}{F_2(\vec{w}, 0)}$$

depend very slowly on the Fourier variable \vec{w} within the phase-matching bandwidth, where they remain close to their peak value attained at $D(\vec{w}) = 0$. Therefore, one can approximately set:

$$\begin{aligned} \frac{F_1(\vec{w}, \vec{\xi})F_2(-\vec{w}, \vec{\xi})}{F_1(\vec{w}, 0)F_2(-\vec{w}, 0)} &\rightarrow \frac{\cosh[g\alpha_p(\vec{\xi})] \sinh[g\alpha_p(\vec{\xi})]}{\cosh g \sinh g} := F_{\text{corr}}(\vec{\xi}) \\ \frac{|F_2(\vec{w}, \vec{\xi})|^2}{|F_2(\vec{w}, 0)|^2} &\rightarrow \frac{\sinh^2[g\alpha_p(\vec{\xi})]}{\sinh^2 g} = F_{\text{coh}}(\vec{\xi}) \end{aligned} \quad (\text{S21})$$

We have tested the validity of this approximation in several conditions: Fig. S4 reports an example of the ratios (S21), plotted as functions of Ω in the central part of the spectrum at $q = 0$, and for $x = y = 0$, in the case of a BBO cut for collinear and degenerate phase matching (parameters as in Fig.S1). When time (or equivalently the spatial coordinate) is chosen well inside the pump pulse

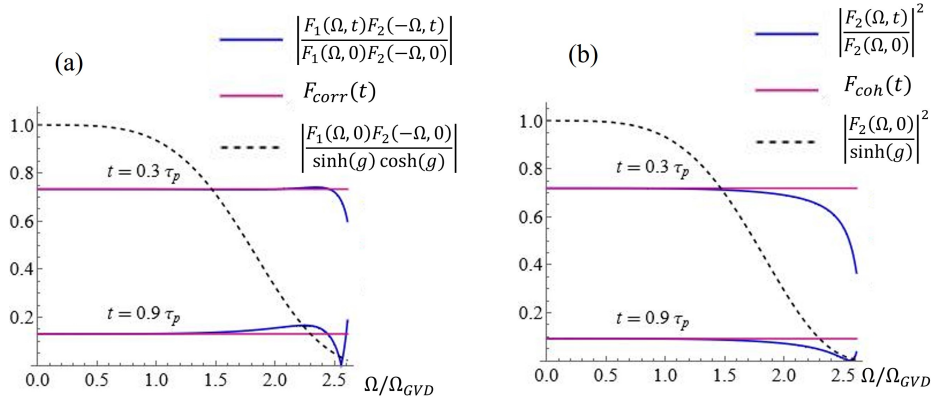


Figure S4. The blue solid lines plot the ratio (S21) as functions of Ω in the central part of the spectrum at $q = 0$, and for $x = y = 0$, for two values of the temporal coordinate, showing that they are almost constant, and equal to their approximated value F_{corr} (a) or F_{coh} (b) (purple). The dashed lines plot for comparison the corresponding spectral distributions (normalized to their peak value). In this example $g = 1.8$, and other parameters are those of a 2mm BBO crystal, cut for collinear phase matching at 1030nm, as in Fig. S1.

profile, the approximation is almost perfect for $F_1 F_2$ (panel a) and slightly worse for F_2^2 (panel b). At larger times along the pump profile, the error made is more consistent, but obviously these points do not contribute much because the fluorescence pulse has there a low intensity.

Fig. S5 reports directly the error made when one substitutes

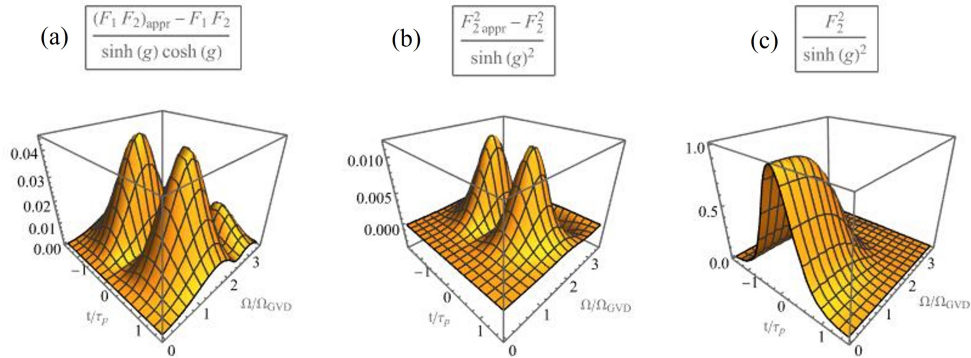


Figure S5. (a) and (b): Error made when substituting the true kernels of the Bogoliubov transformation(1.17) with their factorized form defined by Eq.(S22). (c) for comparison shows $F_2(\vec{w}, \vec{\xi})^2$. All the functions are plotted as functions of Ω and t for $q = 0$ and $x = y = 0$, and are scaled to their peak values. $g = 1.8$, other parameters as in Fig. S1.

$$\begin{aligned}
 F_1(\vec{w}, \vec{\xi}) F_2(-\vec{w}, \vec{\xi}) &\rightarrow \left(F_1(\vec{w}, \vec{\xi}) F_2(-\vec{w}, \vec{\xi}) \right)_{\text{appr}} = F_{corr}(\vec{\xi}) F_1(\vec{w}, 0) F_2(-\vec{w}, 0), \\
 F_2(\vec{w}, \vec{\xi})^2 &\rightarrow \left(F_2(\vec{w}, \vec{\xi})^2 \right)_{\text{appr}} = F_{coh}(\vec{\xi}) F_2(\vec{w}, 0)^2
 \end{aligned} \tag{S22}$$

Fig. S6, finally, illustrates the validity of the approximation in the space-time domain [panels (a) and (b)], and in the spectral domain [panels (c) and (d)]. (a) and (b) compare the temporal shape of the distributions $F_{corr}(0, t)$ and $F_{coh}(0, t)$ resulting from the factorized model (1.23) (purple lines), with the corresponding ratios calculated in the model (1.19) at two different

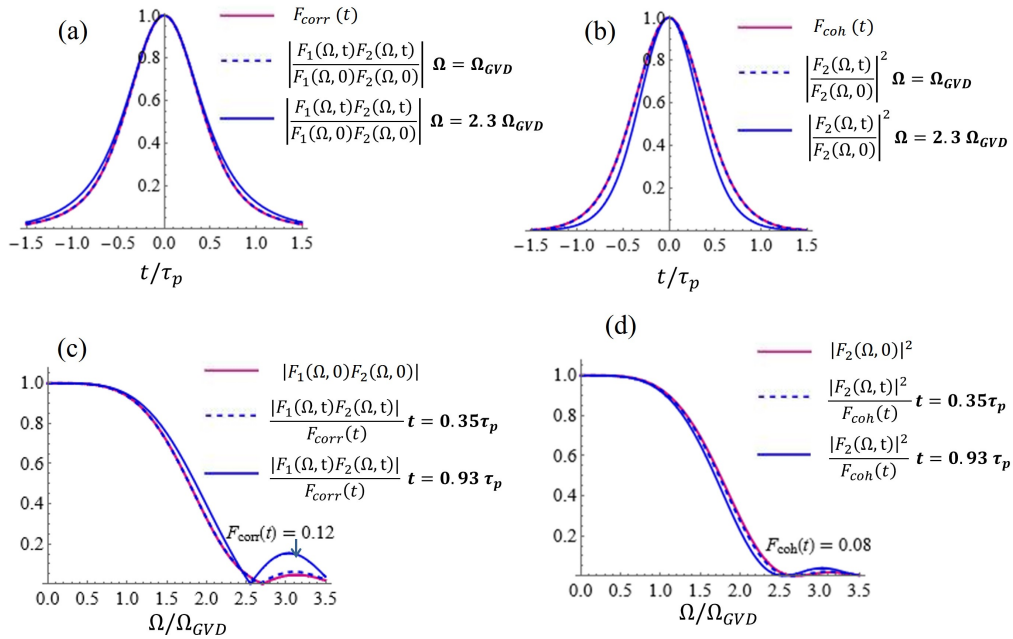


Figure S6. The plots illustrates the validity of the approximation (S21) in the space-time domain (a) and (b), and in the spectral domain (c) and (d), see text. $g = 1.8$, other parameters as in Fig. S1.

Fourier coordinates (dashed blue curve: $\Omega = \Omega_{GVD}$, $q = 0$, solid blue curve $\Omega = 2.3\Omega_{GVD}$, $q = 0$), and shows again that the approximation is excellent when the Fourier mode is chosen well inside the phase-matching bandwidth, and become slightly worse at the bandwidth borders. Panels (c) and (d) are the corresponding spectral counterparts, with red lines showing the approximated result of the factorized model of Eqs.(1.23) and the blue lines plotting instead the corresponding quantities calculated with the less approximated model (1.23). In these examples the gain is intermediate $g = 1.8$, and we checked that the results appear definitely better for low gain $g < 1$, while we did not notice significant differences at higher gain.

With this approximation, the correlation and coherence functions take the factorized forms of Eqs.(1.23), which for example for the biphoton correlation $\Psi(\vec{w}, \vec{w}')$ is the product of a fast decaying correlation peak, function of the distance $\vec{w}_0 = \vec{w}' + \vec{w}$ and a slowly varying function of \vec{w} . This form is very advantageous for analytical calculations, but as already remarked, when more precise quantitative evaluations are needed, the less approximated form (1.19) of results can be instead used and numerically evaluated.